UNIVERSITÀ DEGLI STUDI DI MILANO-BICOCCA

DIPARTIMENTO DI SCIENZA DEI MATERIALI

Scuola di dottorato in Nanostrutture e Nanotecnologie
XXIII ciclo

Top-down and bottom-up approach to self-assemble multifunctional porous films.

Supervisor: Prof. Leo Miglio
Co-Supervisor: Prof. Plinio Innocenzi

Dottoranda:
Daniela Marongiu

Dicembre 2010

Contents

Abstract

A double simultaneous approach has been used in this doctorate work in order to obtain complex multi-functional porous materials which can find application in bio-senors and lab-on-a-chip devices. On one side a method to achieve an increase in the biological analyte detection within the mesoporous films has been studied through the application of deep x-ray lithography. This technique causes multiple effects on the film allowing to easily obtain the final desired structure. On the other hand, wider pores than mesopores are required for the use of thin films as a host for biological species, both due to the size requirement and for the easier pores accessibility by mean of larger pores. The possibility to tune important parameters such as pore size and shape and pore accessibility or selectivity has been achieved in this work thus giving rise to multi-functional macro-mesoporous materials in form of thin films.

Introduction

Nanomaterials usually exhibit physical and chemical properties different from the bulk, as a consequence of their having at least one spatial dimension in the size range of 1±100 nm [1]. Bulk materials can be remodeled as nanomaterials in two main ways through a bottom-up and a top-down approach: the first by providing them with nanoscale porosity and the second by reducing one of their physical dimensions to the nanoscale. Bottom-up nanofabrication of materials that self-assemble into well-defined morphologies, shapes, and patterns is a leading trend in nanotechnologies. Integration of nano- and microfabrication techniques with bottom-up and top-down processing of materials is an important goal for basic and applied research such as for practical exploitation in devices.

The aim of the work reported in this thesis is to explore further approaches in the construction of porous materials in the form of thin films. Mesoporous silica films (i.e. with pore size in the range 2-50 nm) have been taken as a starting point for the development of new hierarchical (i.e. with at lest two order of magnitude of pores) thin films for nano-biological applications by lab-on-chip devices. The directing factor during the whole work was to find the easiest way to achieve this goal by approaches never taken into account before. The final material should be able to play host to biological species possibly in a selective way in order to use different pores for different functions. The main characteristics required for these applications are biocompatibility, accessibility of pores for a post grafting approach and tunable pore size and shape. Also high reproducibility is an important task to be fulfill. The strategy to fabricate new advanced devices that can utilize sol-gel materials for applications in biotechnology or complex smart platforms such as lab-on-a-chip is the use of a controlled process that combines sol-gel

synthesis and deep X-ray lithography (DXRL) offering a facile design and production of miniaturized devices. Even if DXRL requires highly brilliant sources such as synchrotron light, the technique shows some distinctive advantages with respect to other lithographic technologies, such as the possibility of fabricating high aspect ratio structures of very good quality and small surface roughness. This technique, already developed by our group [2], has been extended in this work to produce functional nanomaterials containing metal nanoparticles. In particular complex patterned microstructures formed by gold nanoparticles embedded in a mesoporous matrix have been obtained with an excellent reproducibility. The fabrication of gold-doped arrays of high surface area can find a direct application as optical transducers for analytical techniques focused on biological detection such as surface plasmon resonance and surface enhanced Raman scattering spectroscopy.

This thesis is organized in four wide chapters as follows:

Chapter 1 shows an overview about porous materials. Also the different approaches used in order to obtain thin porous silica films with interesting peculiarities are reported. In particular the evaporation-induced self-assembly (EISA) process and the dip-coating deposition technique are fully explained as the basic way to obtain mesoporous thin films in this work. Further improvements in this techniques give the starting point to the subsequent experiments always focused on solvent evaporation. Deep X-ray lithography is reported as a technique able to fulfill, other than film patterning, a double simultaneous function: formation of nano-objects in the silica film starting from a precursor and densification of the mesoporous silica matrix.

Chapter 2 describes the most utilized characterization techniques for the study and analysis of the samples both in the chemical and in the physical point of view. Instruments are summarized in the basic working principles giving a more detailed explanation of the importance and advantage of the technique in analyzed samples.

In *Chapter 3* all the experimental results are reported. It is the longest and most important chapter. It explains in details the experiments with the most significant results obtained. The direct application of a deep X-ray lithography

is used not just as a patterning technique for mesoporous thin films but in order to achieve the formation of metal (in particular, gold) nanoparticles within the mesoporous matrix, thus giving rise to surface enhanced Raman spectroscopy. On the other hand the preparation of hierarchical thin silica films through a new, very easy and highly reproducible one-pot synthesis route is reported as a way to produce multi-functional materials by selective pores opening. A step ahead in the obtaining of selective porousity is then given by the study of phase separation in aged solutions. This procedure allows to obtain a porous thin film with pores originated by two different phenomena. Such pores have the same order of magnitude but they can be selectively used with different functions;

Last *Chapter* shows the conclusions we can draw up to this time. A short summary of the work is reported with the future perspective.

Chapter 1

How to design multi-functional materials

1.1 Bottom-up and top-down approach

Bottom-up syntheses involve the assembly of small (generally atomic or molecular) units into the desired structure. The wide variety of approaches aiming the achieving of this goal can be split into three categories: chemical synthesis, self-assembly and positional assembly. In the bottom-up route, nano to microscale patterned structures are assembled using interactions between molecules or colloidal particles. The strategies for the synthesis of nanomaterials using bottom-up approaches involve the assembly of small units, also called nanobuilding blocks (NBBs) into a nanostructure, where the NBBs are arranged according to a well-defined shape and architecture. Self assembly is a bottom-up production technique in which atoms or molecules arrange themselves into ordered nanoscale structures by physical or chemical interactions between the units.

Top-down manufacturing involves starting with a larger piece of material and reduce its dimensions by chemical etching, milling or machining, until a nanomaterial is obtained from it by removing material. This can be done by using techniques such as precision engineering and lithography. Top-down lithographic approaches offer arbitrary geometrical designs and good nanometer-level precision and accuracy. Lithography in general involves the patterning of a surface

through exposure to light, ions or electrons, and then subsequent etching and deposition of material on to that surface to produce the desired device.

Mesoporous and mesostructured materials, in the form of films, are an important bottom-up example of porous materials for nanotechnology. The combination of sol-gel and supramolecular chemistry allows the creation of complex systems that self-assemble into organized structures. The formation process of these films is generally well described in terms of evaporation-induced self-assembly (EISA) but the development of micro- and nanofabrication technologies is necessary for a practical application of these materials. The nanofabrication process gives the ability of patterning structures below 100 nm; above this limit, the process can be classified as microfabrication [3].

Since both top-down and bottom-up approaches have advantages and drawbacks, it is not possible to determine which is the best synthetic strategy to obtain the final desired structure. However, the possibility of building structures defined at the atomic or molecular level is a prerogative of bottom-up syntheses, whereas complex structures such as micro- and nanoscopic interconnects and circuits can be obtained by top-down approaches. This consideration shows the potential of hybrid bottom-up and top-down syntheses [4].

1.2 Mesoporous materials

According to IUPAC recommendations [5], nanoporous solids fall into three categories depending on the pore sizes: materials with pore free diameters of less than 2 nm are called microporous, those with pores in the range of 2 to 50 nm mesoporous, and with pores over 50 nm macroporous. Microporous and mesoporous materials are generally referred to as nanoporous materials, which fall into the general class of nanostructured materials, since they possess features (pores) which are defined on the nanoscale. Porous materials find their historical applications in catalysis, filtration, extraction, cleaning and sorption. In the past years, one of the major limitations to be solved was the size and accessibility of pores, which were limited to the sub-nanometer scale in molecular sieves such as natural and synthetic zeolites. The discovery of mesoporous silica with ordered pore

arrangement and tunable pore size in the range 2-50 nanometers constituted a starting point for new porous materials for advanced applications such as sensing and electronics.

Because of the controlled tunability of porousity at the mesoscale and well-defined textures and morphologies (for example, in a variety of inorganic materials, polymers and carbon compounds) mesoporous materials present a unique opportunity to create a new generation of materials that may be used as films for thin-layer chromatography, as separation membranes or as micron scale elements for lab-on-chip analysis systems [6]. In addition, ordered mesoporous materials have potential applications in several fields such as size- and shape-selective separations, adsorption, and immobilization of proteins and other biological molecules and as hosts for functional organic molecules or nanoparticles. The use of porous materials with large internal surface area is a promising strategy also for constructing biosensing devices. Compared to many traditional sensors with limited surface area, porous sensors offer large improvements in device sensitivity.

In particular, the synthesis of mesoporous materials in the form of homogeneous thin films, was a very important achievement because it allowed the development of materials for advanced applications, e.g. in optics, sensing and microelectronics. Thin films of ordered metal oxides and semiconductors find applications in areas such as photovoltaics, gas sensing, thermo electrics, and low-k dielectrics [7][8][9].

An example of mesoporous material is represented by materials obtained through self-assembly of supra molecular templates which is at the base of the bottom-up fabrication method among nanotechnologies. Self-assembly is a well-known general phenomenon used in nanoscience to produce ordered structures by mean of well-defined nano-objects. The general phenomenon is commonly indicated as evaporation-induced self-assembly (EISA) [10] (see section 1.3.1). The creation of these materials with complex and perfect organization at the mesoscale implies, essentially, a combination between the sol-gel chemistry of the precursors (alkoxides, organoalkoxides, salts etc.) and the self-assembly features of the pore templates (typically surfactants). The understanding of the chemical concepts related to these two fields is fundamental to produce the appropriate

nano building blocks (NBBs) that will build up the mesostructures (structure obtained through a micelles templating self-assembling process), and to control the complex assembly processes between them. Sol-gel processing, based on the controlled polymerization of molecular oxide precursors in mild temperature conditions, organic solvents, and controlled amounts of water is crucial in the development of synthesis routes of the NBBs. Oxide formation through the sol-gel process implies connecting the metal or metalloid (Si, Ge) centers with oxo or hydroxo bridges, therefore generating metal-oxo or metal-hydroxo polymers in solution. Hydrolysis of an alkoxy group attached to a metal or metalloid center leads to hydroxyl-metal species which can react with other metal centers leading to condensation reactions, in which an oligomer is formed by bridging two metal or metalloid centers. Condensation can lead to an oxo bridge, and water or alcohol is eliminated as extensively explained in section 1.3. In EISA, the evaporation of the solvent, in presence of a pore template such a surfactant, drives the formation and organization of micelles, while polycondensation reaction of precursors, whether inorganic or organic, at the micelles surface forms the mesostructure matrix. The process is not a simple evaporation of a solutions because the solvent evaporation is a very fast phenomenon and the kinetics are critical. It is therefore based on the control of several chemical parameters such as initial sol composition, pH and aging time, and processing ones such as relative humidity and temperature. Self-organizing porous materials provides simple and low-cost processes to make large-area periodic nanostructures.

Non-ionic amphiphilic block copolymers or ionic surfactants are currently used to direct the formation of the mesostructure in the films. Block copolymers in particular are well-known examples of self-assembling systems, in which chemically distinct blocks microphase separate into nanoscale periodic domains. The final removal of such surfactant, acting as pore templates, gives rise to an open porousity within the material.

A great number of characteristics, including framework nature (composition, crystalline structure and crystallite size), high surface area, pore dimension, shape, surface, accessibility, pore array symmetry and interconnection can be tailored, and even tuned, by a strict control of synthesis steps. These materi-

als present an increasing interest and potential in several fields in which a large functional interfacial area contained in a robust framework is required (e.g., for exchangers, (bio)catalysts, nanocomposites for energy applications, etc.).

With regard to bio-nanotechnology, nanometric to submicrometric pore sizes are interesting for the interaction with proteins, polynucleotides or for the inclusion of a variety of biological nanostructures (enzymatic systems and liposomes to cell membranes and ion channels). Moreover the possibility of creating mesoporous hybrid materials in the form of thin films is of special interest, for the combined properties of a tailored pore system and the inherent features of thin films (i.e., accurate control of thickness, composition, transparency, possibility of multilayer stacking etc.). Mesoporous hybrid organic-inorganic thin films have their historic direct application in ultra low k dielectrics and low refractive index materials with a good mechanical stability and a hydrophobic nature. Anyway the ability of shaping mesoporous materials as thin films leads to other applications, such as sensors, delivery devices or controlled bioceramics. In the first case, 100-500 nm thick films with accessible porosity should allow a rapid transit of analytes, drugs, signal or trigger molecules across nanomembranes. Film-processing procedures allow the stacking of thin films with different characteristics, thus leading to multilayer systems, each layer possessing a peculiar chemical property located in a well-defined position in space. Transparent films containing light-responsive functions can be combined with nonlinear optical chromophores to produce multifunctional photonic devices [11].

The preparation of mesoporous silica took its origin from the pioneer works by Mobil on surfactant-templated materials designated as MCM-41 [12]. They reported the synthesis of mesoporous solids from the calcination of aluminosilicate gels in the presence of surfactants. The material showed regular arrays of uniform channels having the dimension in the range of 16 to 100 Å which can be tailored through the choice of surfactant and the reaction conditions. Transparent thin films of layered silica-surfactant nanocomposites by polymerization of tetramethoxysilane in aqueous solutions of alkyltrimethylammonium salts is first reported by Ogawa in 1994 [13]. The composites were obtained as oriented transparent films creating a new class of materials for molecularly designed self-

assembly. The silica film deposition was then reported by Ozin's group [14][15] describing the synthesis of thin ordered films of mesoporous silica grown on freshly cleaved mica at mica-water interface. The surface structure and reactivity of the mica substrate controls the orientation of micellar precursor species. Then the group described that such films can be grown without a solid substrate, by surfactant templating at the interface between air and water. Later Brinker's group [10][16] summarized a simple evaporation-induced self-assembly process, that enables the rapid production of patterned porous or nanocomposite materials in the form of films, fibers, or powders. This procedure allows the material in the shape of powders (aerosols [16]), gels, monoliths [17][18][19][20][21] or films to be processed.

1.3 Self-assembled mesoporous thin films

The most broadly and extensively investigated composition for mesoporous thin film is pure silica, SiO_2, mainly due to its strong tendency to form a gel with different precursor sols. Silicon alkoxide has been a major choice for the starting material, and its extraordinary slow hydrolysis kinetics allowed to analyze in detail the whole process of sol formation, polycondensation and gel formation, by means of various techniques such as infrared spectroscopy, for the understanding of the phenomenon in the molecular scale, as well as the x-ray scattering for larger scale structures. The deposition of the film is typically done by spin-coating or dip-coating. The dip-coating technique, used during this work, (see section 1.3.2) offers a large number of chemical and processing parameters to experiment with such as humidity and temperature. Because evaporation takes place in a very short period of time and the quantity of material is very low because film thicknesses are lower than 1 μm, such systems are difficult to investigate. However, characterization of the films can be achieved by combining several techniques such as Fourier transform infrared spectroscopy, ellipsometry, X-ray diffraction, grazing incidence small-angle X-ray scattering, transmission electron microscopy and atomic force microscopy.

Mesoporous silica thin films are obtained by the sol-gel method and the dip or

spin-coating deposition process starting from Si precursors. Sol-gel processing is a low temperature synthesis route spread in several field of applications. Its high versatility makes it particularly suitable to obtain good quality thin films from a liquid phase. The precursor is either an alkoxide, i.e. a compound where a metal (e.g. Ti, B, Al, Ga, Zr, Y, Ca) or metalloid (Si, Ge) is chemically bonded to one or more organic groups through an oxygen atom, or an inorganic salt, generally a transition metal chloride. Silicon alkoxides $Si(OR)_4$ such as tetraethoxysilane (TEOS) are widely used in order to produce silicon oxide (silica). Typically the alkoxide is used with the corresponding alcoholic solution, such as ethanol in case of TEOS and MTES.

As an example, the sol-gel processing of TEOS is reported. This alkoxide is constituted by a Si atom bonded to 4 ethoxy groups which are hydrolyzed in the presence of water, an alcohol and a catalyst such as HCl.

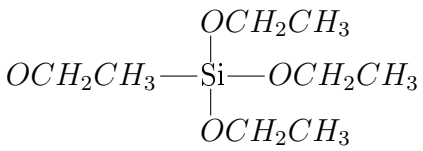

These, in turn, condense with other hydrolyzed species and with unhydrolyzed TEOS molecules, forming a larger macromolecule and yielding smaller molecules such as water or ethanol. Therefore, Si atoms end up linked by bridging oxygens or hydroxides in a SiO_4 network.

The sol-gel transition of a metal or metalloid alkoxide solution is generally caused by two kinds of reactions, such as hydrolysis and polycondensation. Although the former one is necessary for the latter to take place, these reactions are known to proceed in parallel from a very early stage of the whole reaction. In usual cases, the hydrolysis is initiated by mixing water with alkoxide in the presence of alcohol as a co-solvent. The hydrolysis of M-OR produces M-OH which subsequently condenses with other M-OH to produce water and a polycondensed species containing an M-O-M linkage. Further condensations lead to the growth of metaloxane oligomers which subsequently link together to form a gel network. The overall reactions for silicon alkoxide, $Si(OR)_4$ are reported in Figure 1.1.

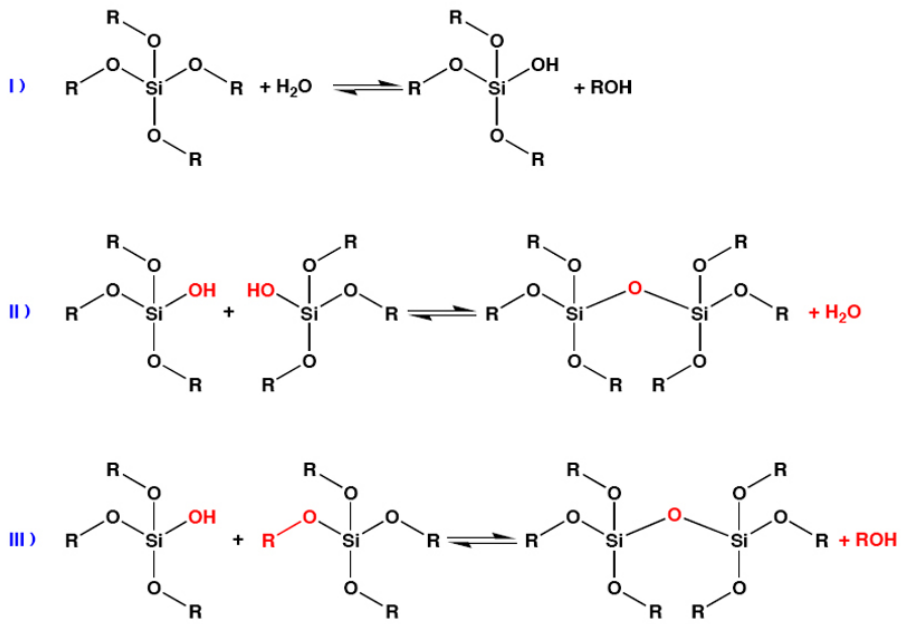

Fig. 1.1: Scheme of reactions for silicon alkoxide.

The overall kinetics of reactions depend strongly on the water concentration, the kind of alkoxy groups and also on the kind and concentration of the catalyst. The following reaction increases the number of M-O-M bonds and consequently the viscosity. Since this condensation process results in the assembly of a macromolecule starting from monomer units, the smaller molecules, such as water and ethanol, link to the forming structure. The resulting material framework can be purely inorganic or hybrid organic-inorganic as in the case of hybrid precursors.

Silicon alkoxides exhibit extraordinarily slow hydrolysis and polycondensation kinetics compared with alkoxides of other kind of metals such as Ti, Zr, B and Al. The polycondensation around the isoelectric point of amorphous silica, pH $\sim$ 2-3 is the slowest, and becomes shorter toward both directions of the pH axis [22]. A controlled hydrolysis of silicon alkoxides is easy and the silica gel materials can be processed into various shapes such as a fiber by spinning a viscous sol, a film by dipping a substrate in a less viscous sol and a bulk by casting a sol and allowing it to gel in a mold.

Catalysts, either acidic or basic, are used to increase the reaction rate. Hydrolysis rate depends on several parameters as molar ratio between water and alkoxide or the nature of R groups and in a neutral environment it is pretty slow. Acidic catalysis promotes the hydrolysis while a basic catalysis increases the condensation rate. In this work acid catalysts were used to promote the reaction.

In order to obtain higher quality films by increasing the degree of order, a precursor solution of TEOS with a hybrid precursor, that is methyl-triethoxysilane (MTES) has been used during this work [23]. MTES has three hydrolysable ethoxy (OCH_2CH_3) groups and a non-hydrolysable CH_3 group which is covalently bonded to the central Si atom.

1.3.1 EISA Evaporation-induced self-assembly

The so-called EISA process, initially proposed by Brinker and colleagues [10] is based on the processes that take place during the formation of mesostructured silica films [24][25][26]. A general definition of self-assembly is the spontaneous organization of chemical entities through interactions as hydrogen bonding, Van der Waals forces or electrostatic forces, with no external intervention. Self-assembly typically employs molecules free to organize into well-defined supramolecular assemblies. Most common are surfactants, amphiphilic molecules or polymers composed of hydrophobic and hydrophilic parts. It is well-known that amphiphilic molecules in water solution can form a variety of supramolecular aggregates (spherical, cylindrical, lamellar, etc.) arranged in ordered structures with different symmetries (cubic, hexagonal, gyroid, etc.). Their symmetries and morphologies show a strong dependence on solution parameters such as pH or electrolyte concentration. At low concentration, amphiphilic molecules in an aqueous solvent are present as free molecules. When the concentration is raised above the critical micellar concentration (cmc), the molecules self-assemble into micelles with a well-defined shape and aggregation number (i.e. average number of molecules per aggregate). At higher concentrations a series of phase transformations may take place, related to changes in the curvature radius of the micelles. This phase transitions follow a general sequence with increasing concentration: direct spheres, direct cylinders, lamellae, inverse cylinders and inverse spheres (see Figure 1.2).

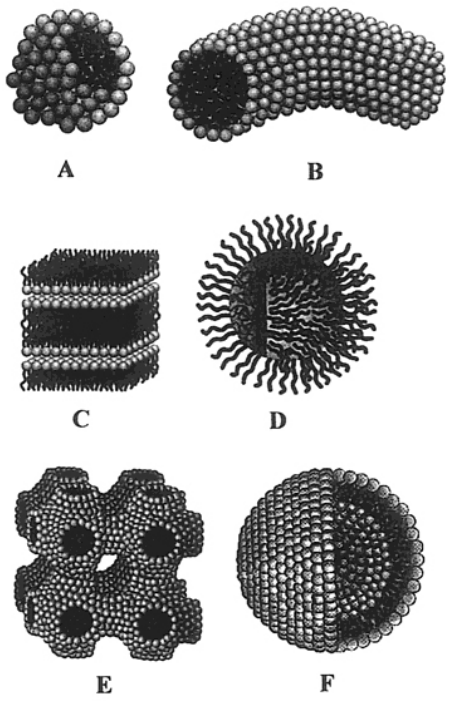

Fig. 1.2: Examples of micellar structures: (A) sphere, (B) cylinder, (C) planar bilayer, (D) reverse micelle, (E) bicontinuous phase, (F) liposomes. Reproduced from Soler-Illia et al. [27]

Micelles in a polar solvent are constituted by a finite number of amphiphilic units in which the hydrophobic regions form the core of the micelle, whereas the hydrophilic ends point towards the exterior and are swelled by solvent molecules (in an apolar medium it is the opposite: hydrophilic cores are surrounded by a hydrophobic ring). In fact in aqueous solution above the critical micelle concentration, surfactants assemble into micelles of different shapes leaving the hydrophilic parts of the molecule in contact with water while shielding the hydrophobic parts within the micellar core as shown in Figure 1.3. Micelle shape is determined by the interactions between the amphiphilic units and the solvent molecules. For high concentrations, micelles can form periodic ordered patterns.

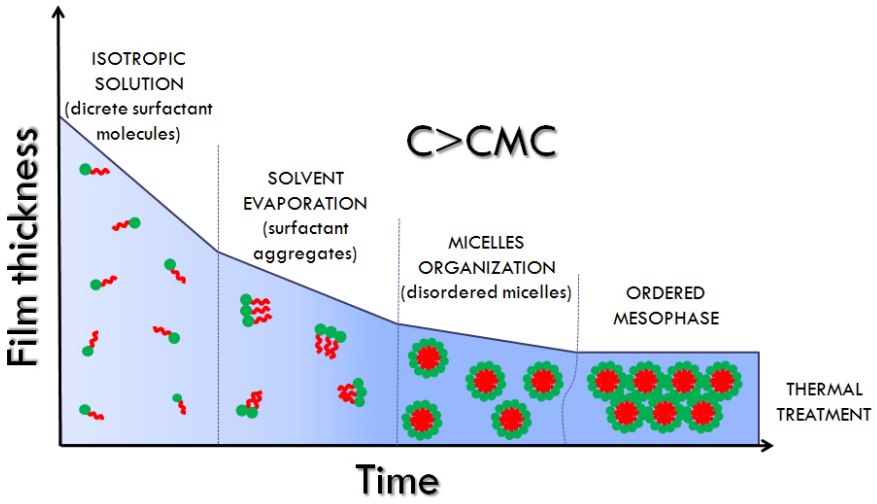

Fig. 1.3: Scheme of the formation of a mesostructured film by evaporation-induced self-assembly. In the isotropic solution condensation is slowed down and the nonvolatile precursors are free surfactant molecules. The subsequent solvent evaporation triggers the formation of surfactant-inorganic units. When the evaporation is complete, the film equilibrates its water content with the environment giving rise to an ordered mesophase. The final thermal treatment stabilizes the mesostructure.

During the dip-coating deposition of an homogeneous solution of soluble silica and surfactant prepared in ethanol/water solvent with concentration $\ll$ cmc, the preferential evaporation of ethanol concentrates the depositing film in water and nonvolatile surfactant and silica species. The progressively increasing

of surfactant concentration drives the self-organization of micelles into periodic mesophases. The result is a rapid formation of thin film mesophases that are highly oriented with respect to the substrate surface. Typically, self-assembled materials show very high-symmetry structures as cubic, hexagonal or lamellar. For silicates this is achieved under acidic conditions close to the isoelectric point of colloidal silica.

1.3.2 The dip-coating deposition

Mesoporous films are typically produced after evaporation of solutions containing an inorganic precursor (alkoxide, chloride or mixtures of both), an organic supramolecular template (mostly ionic, nonionic or polymeric surfactants) and some additives (in general, acidic or complexing molecules to control pH, thus avoiding inorganic extended condensation) dissolved in a volatile solvent (mostly low boiling point alcohols). Deposition techniques are different: from controlled drying of deposited droplets to dip- or spin-coating. EISA is most often used in combination with the dip-coating deposition technique (or, less frequently, with spin-coating). The deposition environment, the evaporation process and the resulting film thickness are important not only for the formation of porosity, but also for the symmetry of the pore array. The complex processes taking place during solvent evaporation and subsequent formation of an inorganic-template organized mesophase is explained in the next section. In this work the dip-coating deposition process has been used. The dip-coating is a rapid ($\sim$ 10 s), dynamic self-assembly process with a steady and continuous nature. These characteristics promote continuous accretion of micellar species onto interfacially organized mesostructures. In dip-coating, a substrate is dipped into the solution and extracted at a constant speed. Due to the solution-substrate wettability, a liquid layer is formed on the substrate, whose thickness depends on the extraction speed (pulling rate) and the viscosity of the solution. As the solvent evaporates from the liquid layer, the inorganic precursors undergo condensation and crosslinking processes, thus forming a gel, which can be defined as a phase constituted by a more or less condensed inorganic network within which residual solvent molecules form an interconnected liquid phase.

The process can be divided in five stages represented in Figure 1.4: immersion, start-up, deposition, drainage, and evaporation [28]. With volatile solvents, such as low boiling point alcohol, evaporation normally accompanies the start-up, deposition, and drainage steps.

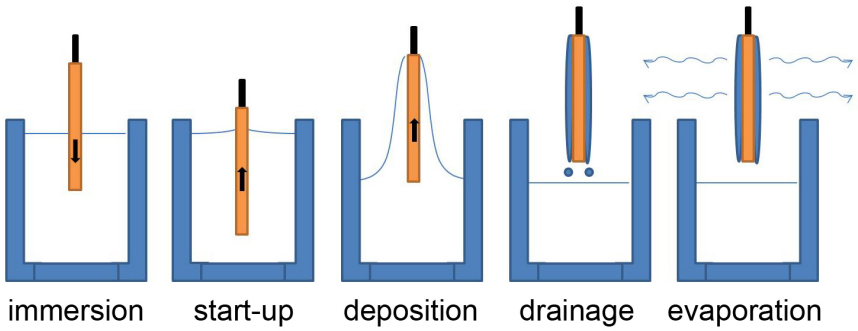

Fig. 1.4: The five stages of dip-coating process.

After the process, deposited films are optically transparent and completely featureless on the micrometer-length scale.

1.3.3 Critical process parameters

Solution preparation and deposition conditions are critical parameters that have to be analyzed and controlled in a strict way. Silicate gels are usually synthesized by hydrolyzing tetrafunctional alkoxide precursors with an acidic or basic catalyst. The hydrolysis reaction replaces alkoxide groups (OR) with hydroxyl groups (OH). Subsequent condensation reactions involving silanol groups produce siloxane bonds (Si-O-Si) plus alcohol or water. Under most conditions, condensation begins before hydrolysis is complete. The water/alkoxide ratio is important to achieve a different products as bulk gels, films, fibers and powders. Theoretically a molar ratio equal 2 is enough to complete hydrolysis and condensation but in fact even in excess water the reaction does not complete. In acid-catalyzed reactions, the molar ratio $H_2O : Si \leq 2$ leads to a gel with lower crosslinking density, which are suitable to form gel fibers and coating films. A substantial amount of

unreacted alkoxy groups tend to remain in the gel network. On the other hand a molar ratio $H_2O : Si \geq 4$ drives to a gel with higher crosslinking density, which exhibit higher tendency to remain monolithic when dried carefully.

Thermal treatment

The final thermal treatment is the last important step in the creation of a mesoporous material. It has the double purpose of promoting inorganic condensation by removing the residual solvent and decomposing the organic components in order to empty the mesopores achieving the calcination. Typically, mild treatments with thermal ramps and steps are preferred: rapid heating at high temperatures may cause mechanical stress in the sample which can damage the mesostructure and lead to macroscopic cracking. The calcination process gives rise to a phenomenon known as thermal shrinkage which changes the shape of mesopores: the contraction occurs in the deposited films exclusively along the direction perpendicular to the substrate (out of plane), whereas the contraction parallel to the substrate (in plane) is negligible.

1.4 Hierarchical porous materials

Pore dimension is another critical parameter for practical application of porous films. Obtaining a material with larger pores or pores with different size and shape is a challenging topic in material science due to the possibility of integrate different functions in different pores. A porous material containing at least two order of magnitude of porousity, from a few nanometers up to micrometer, is called hierarchical porous material. Hierarchical porous structures, presenting pores with different sizes and functions, represent a natural evolution of advanced mesoporous materials. Hierarchical porous films allow much higher overall porosities (easily up to 90-95%) than crystal-like systems, while preserving the structural integrity. Hierarchy is a defining feature of self-assembly that is appreciated in biology due to the possibility of building multi-functional materials. The possibility to obtain such hierarchical structures through one-pot assembly processes is an important achievement in this field. The common way to build hierarchically

porous films is related to a combination of techniques such as the combined use of micromolding, latex beads, and surfactant templating [29]. Macro and mesoporous films can also be obtained by the sol-gel method together with a phase separation process [30]. In an alternative route, hierarchical thin films can be obtained by a combination of aging and phase separation; in this case macropores arise from phase separation, and small-size mesopores <10 nm are generated by a self-assembly process using a typical organic block copolymers as templates in the sol-gel matrix. Following this idea, it is also possible to obtain a porous material in which pores of the same average size are originated by different phenomena giving rise to an interesting material presenting a pore selectivity (see section 3.3.1).

Different types of hierarchical porousity are possible depending on the pore dimensions involved in the porous structure such as micro-meso, meso-macro or micro-macro for a bimodal distribution. In general, two main approaches are envisaged, based on the introduction of macrotemplates (with size ranging from 100 nm to several micrometers: latex or silica nanoparticles, large polymers, bacteria, etc.) directly in the reaction media or by combining these macrotemplates with usual mesoscale templates (surfactants, molecular agents, etc.). Materials presenting multimodal or multiscale porosity present a major interest, particularly for catalysis and separation processes, where optimization of the diffusion and confinement regimes is required. Whereas micro- and mesopores provide the size and shape selectivity for the guest molecules, enhancing the host-guest interactions, the presence of macroporous channels should allow improved access to the active sites at the immediate smaller scale, avoiding pore blocking by reagents or products.

One of the emerging properties in porous materials is the multifunctionality. In fact, when these materials are able to supply multiple functions they are called multi-functional materials and the hierarchy is fundamental for this purpose. The term hierarchical material describes a complex material composed by different functional objects whose different dimensions play different roles. The importance of such materials with different ranges of porosities consists in their ability to play a different function in each pore scale. Meso-macro materials in particular are

important in biological application such as molecular biosensing of big molecules like proteins.

1.4.1 Strategies

Several strategies can be envisaged for the production of hierarchical porous materials. Mesoporous-macroporous silicas have been obtained in an original and simple way by adjusting sol-gel hydrolysis/condensation kinetics and solvent-mineral polymer interactions [30]. Macroporosity can be controlled by inducing a phase separation between a continuous solvent phase such as a hydrosoluble polymer and a growing inorganic network. Mesoporosity can be controlled by solvent exchange and treatment in alkaline conditions. These silica phases are being developed as chromatographic supports [30]. Segregation of aqueous droplets can also give rise to spongelike membranes, which also display mesopores [31]. Other examples are the use of a sacrificial template such as micelles or polymeric particles of different dimensions which produce pores of the same templates dimensions [32][33] or a patterning technique. One-pot strategies for the synthesis of these materials can be represented by the use of two different templates. In such a way it is possible to obtain hierarchical materials with a controlled interconnection and accessibility of pores.

1.4.2 Pore size

In a porous material the pores can be very uniform in shape and size or can cover a wide range of pore sizes. The wall structure can be highly organized (crystalline) or highly disorganized (amorphous). The synthesis procedure of a porous material must be able to control both pore dimensions and pore size distribution, which are generally required to be narrowly centered on a specific value for practical applications. Advanced applications may require pores that are either interconnected and open to the external environment in order to allow the diffusion of species through the porous material [34], or isolated and not accessible from the outside as in low dielectric constant materials in microelectronics.

1.5 Top-down approaches in mesoporous thin films

Self-assembled mesoporous thin films are an important example of bottom-up synthesized materials for which integration in devices requires top-down processing [35][4]. The ordered mesopores are an ideal host for functional organic molecules or nanoparticles and the patterns, from nano to micrometer scale, allow the design of devices for different types of advanced applications, for example DNA nanoarrays or lab-on-a-chip devices. The possibility to pattern mesoporous films was first demonstrated by Brinker et al., who employed a wide range of lithographic techniques [36][37]. The need for high-tech integrated components requires more and more sophisticated lithographic techniques to achieve higher aspect ratios, a higher definition, the capability to pattern thick structures, higher resolution (depending on film thickness, down to few tens of nanometers). It is important to underline that several of the possible applications that are envisioned for mesoporous materials, such as nano-micro arrays and lab-on-a-chip devices, have exactly these stringent requirements. With this aim Falcaro et al. developed in 2008 a highly integrated fabrication patterning process that is based on deep X-ray lithography [2].

Multi-functional nanostructures need to be fabricated with a specific design and must be compatible with the current lithographic technologies. Top-down lithographic techniques are generally based on application of a writing beam, such as UV light, X-rays, electrons, to a material that responds to the radiation. The writing process can be direct or used for preparing a mold and to pattern through replica. Bottom-up preparation of nanostructured films is more compatible with soft-lithography techniques, but these techniques appear at the moment not well integrated with the current technologies of mass production, which are mainly top-down [38].

The ability to pattern porous thin films is important for a number of technological applications, including sensor arrays and microfluidic devices. In the top-down approach, different types of lithographic techniques are employed to pattern silica mesoporous thin films. Lithographic techniques are commonly

classified in two categories: conventional and unconventional lithographies. This classification is generally based on the level of commercial development of the technique. Photolithography and particle-beam lithography are the most widely used conventional techniques for micropatterning. Molding and scanning-probe lithography are some examples of non conventional methods.

1.5.1 Lithographic techniques

The patterning of mesoporous films is possible by using a wide range of lithographic techniques. Soft lithographic approaches [39] such as contact printing, replica molding or micromolding in capillaries can be used to pattern mesoporous films but they require long processing times or are limited to physically defining the presence or absence of discrete isolated regions [29][40]. Rapid patterning of organofunctionalized mesoporous thin films by means of pen lithography, ink-jet printing, and selective dewetting can also be used but none of them is able to pattern thin-film mesostructure or properties.

Among conventional lithographic techniques for patterning silica mesostructured films, electron-beam lithography (EBL) is widely used. An electron beam resist mold is usually prepared by spinning a resist solution onto a silicon wafer. The resist mold is then patterned by EBL to obtain the desired shapes. The precursor solution is deposited via spin-coating on the patterned molds. After removal of the resist and calcination, patterned mesostructures are obtained. Patterns with a height of 1 μm and a width of 0.25-50 μm could be fabricated by EBL. After EBL polymerization of the organic components occurs, the structure is calcined through a post-exposure thermal treatment. The exposed region becomes insoluble and a negative resist-like behavior is observed. This direct patterning of the films makes the two-step process faster and easier when compared to traditional lithography where a photoresist is required. Use of a focused electron beam makes it possible to delineate fine patterns, although writing of chip-scale patterns with a single electron beam is a slow process [41].

Alternatively to EBL, soft X-ray lithography (SXRL) induces the same reaction on epoxy systems in an equivalent process [42]. Radiation damage is a drawback when X-rays are used to promote crosslinking in the functional mate-

rial; however, the resolution is extremely high since the wavelengths are so small (∼1 nm). On the other hand, deep X-Ray Lithography (DXRL) offers a method to reliably manufacture microstructures with a number of features [43]. Three-dimensional structures have been generated in a thick layer (up to 600 mm) using DXRL, and the process allows fast production of ultra-precise microstructures with extreme aspect ratio [44].

1.5.2 Deep X-Ray Lithography

Deep X-ray lithography is a process by which a material that is exposed to high-resolution, high-intensity, and extremely collimated synchrotron radiation through an X-ray mask changes its dissolution rate in a liquid solvent (developer). The light source wavelength is a critical parameter that determines how small and how deep the patterning can be. Deep X-ray lithography allows the production of high aspect ratio three-dimensional structures in polymethylmethacrylate (PMMA) with quasi perfect side-wall verticality and optical quality roughness. These structures can then be used as templates to mass-produce microparts made out of a large variety of metals, alloys or ceramics. It opens a wide variety of potential application in the field of micro electromechanical systems (MEMs), fiber and integrated optics, microfluidic devices and interconnection technology. By this lithographic technique, the mask pattern is, therefore, transferred to the material.

1.6 A top-down and bottom-up combined approach

There are a wide variety of techniques that are capable of creating nanostructures with various degrees of quality, speed and cost. The two main methods to obtain nano- to microscale patterns are usually characterized as bottom-up and top-down. Mesostructured films have several specific properties that make them a very challenging material to be patterned. It is, in fact, possible to use a top-down lithographic process such as deep X-ray lithography, as a techniques

able to produce a change in the film porous structure. The possibility to obtain patterns of porous materials that also exhibits a highly controlled pore-size distribution and pore topology is of high technological interest because the organized mesopores can be used as hosts for functional organic molecules or nanoparticles which can be used in several types of advanced applications. The lithographic approach on surfactant-templated mesoporous films is based on selective removal of template and silica polycondensation induced by synchrotron radiation. The exposure of the films to X-rays did not cause any structural change in mesophase or damage such as cracking, but the areas of the film that are not exposed to radiation can be selectively etched due to a lower crosslinking degree of the inorganic network. An important advantage of this method is the possibility to simultaneously remove the surfactant and to induce condensation of the silica network in a single-step process together with the patterning process.

1.6.1 Current technology and improvements

Recently deep X-ray lithography (DXRL) has been used to produce microstructures with high aspect ratio even if DXRL requires highly brilliant sources such as synchrotron light, the technique shows some distinctive advantages with respect to other lithographic technologies, such as the already mentioned possibility of fabricating high aspect ratio structures with a very good quality and small surface roughness. High-aspect ratio materials can be easily obtained in a microscale but the potentiality of application of the technique extends to the nanoscale [2]. We decided to follow this approach by implementing this technique with a new functionality useful for a direct practical application of such materials. This technique can be indeed extended to produce functional nanomaterials containing nanoparticles. Sensing and nanobiotechnologies need the quantitative detection of biological species which can be obtained by Raman spectroscopy. In particular surface-enhanced Raman scattering is a method in which analytes are adsorbed on nanoscopically structured metallic surfaces and excited by strong electric fields that are induced by surface plasmon resonance. It has great potential as an analytical tool. Due to an interaction of analyte molecules with a nanostructured metallic surface, the Raman signals get efficiently enhanced up to 11 to 14 orders

of magnitude. Thereby a single molecule detection level is achieved. With this aim the need to fabricate gold-doped arrays of high surface area [45] [46][47].

In this work, deep X-ray lithography has been applied to fabricate complex patterned microstructures formed by gold nanoparticles embedded in a mesoporous matrix through a direct and simple procedure and with a high integration of bottom-up and top-down technologies [48].

Chapter 2

Characerization techniques

The physics and the chemistry related to templated self-assembly in mesostructured films have been understood in detail. Advanced analytical tools and techniques are fundamental for the characterization and monitoring of the thin film structures and properties. The characterization techniques must be able to detect different aspects such as morphology, composition, mesostructure degree of order, presence of specific molecular bonding. Among the techniques widely used, Fourier-transform infrared spectroscopy (FTIR) is always utilized in order to provide informations on the presence of specific chemical species and bondings within the film. A powerful technique for investigating the structure of mesoporous materials is the transmission electron microscopy (TEM), which provides direct images of the mesostructure with nanometric resolution. It gives structural information on thermally treated and mechanically stable samples. Other techniques, such as small-angle X-ray scattering, usually belonging to different field, have been recently adapted to the investigation of porous films.

Because a description of all characterization techniques utilized in the research on porous materials falls outside the scope of this thesis, the present chapter provides information on the main characterization techniques employed in the experimental work of this doctorate. They are briefly described in their physical principles showing mainly the advantage of each of them in the characterization of the obtained porous samples. These can be classified in spectroscopic techniques, yielding physicochemical information on the film (e.g. presence of specific

chemical species, degree of inorganic crosslinking). Structural techniques, giving information on the mesostructure such as symmetry, cell parameter, morphology.

2.1 Spectroscopic analysis

2.1.1 Infrared spectroscopy

Infrared spectroscopy is an important analytical technique which potentially allows the study of any sample in any physical state. The main goal of IR spectroscopic analysis is to determine the chemical functional groups in the sample. This technique is based on the vibrations of the atoms of a molecule. An infrared spectrum is commonly obtained by passing infrared radiation through a sample and determining what fraction of the incident radiation is absorbed at a particular energy. The energy at which any band in an absorption spectrum appears corresponds to the frequency of a vibration of a part of a sample molecule. A significant improvement in the technique is the introduction of Fourier-transform spectrometers [49]. This type of instrument employs an interferometer and takes advantage of the mathematical process of Fourier-transformation making the analysis much faster. Fourier-transform infrared spectroscopy is based on the idea of the interference of radiation between two beams to yield an interferogram. This is a signal produced as a function of the change of pathlength between the two beams. The two domains of distance and frequency are interconvertible by the mathematical method of Fourier-transformation.

The bands that appear can usually be assigned to particular parts of a molecule, producing the group frequencies. The characteristic molecular motions responsible for infrared bands are different in the mid-infrared and far-infrared range. Both these techniques are used in this work.

The mid-infrared spectrum, in the 4000-400 cm^{-1} range, shows the bands related to X-H stretching like O-H, C-H and N-H stretching; the triple-bond like C≡C, the double-bond and the fingerprint; Each band in an infrared spectrum can be assigned to a particular deformation of the molecule, the movement of a group of atoms, or the bending or stretching of a particular bond, however many

vibrations may vary by hundreds of wavenumbers even for similar molecules. A spectrum of a molecule may have a hundred or more absorption bands present, but it can be regarded as a fingerprint of the molecule with no need to assign all the bands. Regarding the porous sol-gel materials, the technique is useful to analyze the degree of hydrolysis and condensation and to study the effect of thermal treatment on chemical bonds.

The far-infrared region is defined as the region between 400 and 100 cm^{-1}. This region is more limited than the mid infrared one, but it provides informations regarding the vibrations of molecules containing heavy atoms, molecular skeleton vibrations, molecular torsions and crystal lattice vibrations.

The instrument used during this work is a Bruker infrared microscope Hyperion 2000 coupled with a Vertex 70 interferometer and optimized for mid-ir (4000-400 cm^{-1}) measurements. While the Bruker Vertex-70v interferometer is the system used to perform Far-Ir spectroscopy (400-30 cm^{-1}).

2.1.2 Ellipsometry

Spectroscopic ellipsometry (SE) is a non-invasive optical technique which can provide thin film structures and properties analysis. Refractive index, percentage of porosity, transparency and dielectric properties can be determined. Ellipsometry is an indirect technique that allows to calculate the unknown parameters such as thickness and film refractive index by fitting the data to a model. This technique uses the change in polarization of light upon reflection from a material to determine the real part (refractive index), $n(\lambda)$ and the imaginary part (extinction coefficient), $k(\lambda)$ of the complex refractive index, of a material, $N(\lambda) = (n(\lambda)+ik(\lambda))$ where λ is the wavelength of the electromagnetic radiation. Linearly polarized light is generally elliptical polarized upon reflection with asymmetric intensity difference ($\tan \Psi$) and phase difference (Δ). The ellipticity, or ratio of minor to major axis of the ellipse, and the orientation of the reflected beam is determined by the relative phase difference Δ and azimuth Ψ (see Figure 2.1. These values are measured using ellipsometry. The ellipticity of the reflected light depends on the optical constants of the thin film and its thickness.

Physical informations about the sample such as film refractive index and thick-

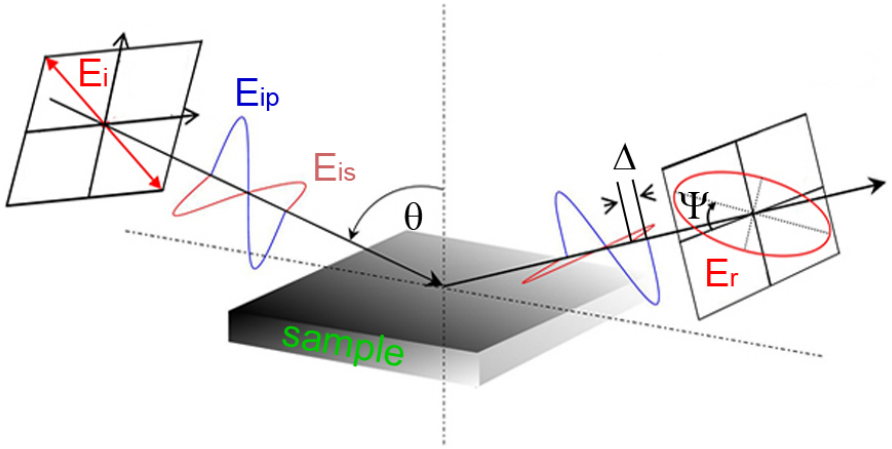

Fig. 2.1: Scheme of ellipsometry principle.

ness are extracted by fitting the spectra to a physical model. The model is built up based on the available information and knowledge of the porous film structure and components of the sample to predict the optical response of the sample to the incident polarized light. For porous thin films usually refractive index, film thickness, porosity and other fit parameters are to be determined. For the sol-gel porous films studied in this work, the optical model used in the fitting of ellipsometric data consists of one or two layers on substrate. Native SiO_2 layer on Si substrate and porous film layer on top or just porous film layers on substrate.

The instrument used in this work is a R-SE Wollam spectroscopic ellipsometer. The ellipsometric spectra analysis is done using CompleteEASE 4.06 software assuming a Cauchy film as fitting model which calculates the refractive index as a function of the wavelength: $n(\lambda) = A + B/\lambda^2 + C/\lambda^4$.

2.2 Structure characterization

2.2.1 X-Ray diffraction

When a beam of x-rays interacts with an arbitrary material its atoms may scatter the rays into all possible directions. In a crystalline solid, however, the atoms

are arranged in a periodic array and this results in a characteristic resulting diffraction pattern. In the Bragg description, x-ray diffraction (XRD) is yield by the constructive interference of waves scattered from successive lattice planes in the crystal. When an incident beam of wave vector **k** hits on a set of lattice planes to form an angle θ with respect to the planes, the angle of deviation between the outgoing and incident rays is $\phi = 2\theta$. The separation between neighboring planes is denoted by d. The Bragg condition is given by $2d\sin\theta = n\lambda$. Constructive interference between successive paths occurs when the path difference equals an integer number of wavelengths.

In mesoporous materials analyzed in this work, mesopores are ordered in a way similar to the atoms in a crystal thus giving rise to a diffraction pattern. The mesostructure peak is at very low angle and it allows the calculation of d-spacing.

The instrument used in this work is a Bruker D8-Discover diffractometer equipped with a Goebel mirror giving a parallel beam. The XRD patterns can be acquired by a scintillator counter or a PSD detector.

2.2.2 Grazing-incidence small-angle X-Ray scattering

The limitations of direct imaging techniques to characterize the morphology of nano-structured materials are represented by the very small observable area and by their lack in ability to determine inner structures of such layers. The small angle X-ray scattering under grazing incident angles (GISAXS) is a very powerful tool in this field. It is a versatile technique for characterizing nanoscale density correlation and it is extreamly useful for the characterization of mesoporous thin films. GISAXS provides information both about lateral and normal ordering at a surface or inside the film. For the investigation of coatings, films and particles on surfaces, the GISAXS method is particularly useful because a highly intense scattering pattern is always obtained, even for films of nanoscale thickness due to the sufficiently long X-ray beam path length through the film plane. GISAXS can be applied to determine internal morphologies of thin films as well as top surface morphologies of films, coatings and substrates.

The geometry of a GISAXS experiment is illustrated in Figure 2.2. A monochromatic X-ray beam with the wavevector k_i is directed on a surface with a very

small incident angle α_i with respect to the surface. The Cartesian z-axis is the normal to the surface plane, the x-axis is the direction along the surface parallel to the beam and the y-axis perpendicular to it. The X-rays are scattered along k_f in the direction $(2\theta_f, \alpha_f)$ by any type of electron density fluctuations at the illuminated portion of the surface.

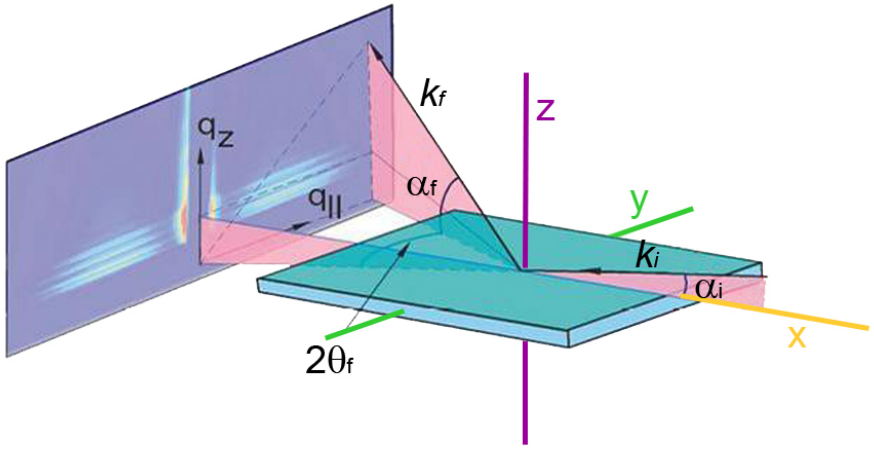

Fig. 2.2: Geometry of a GISAXS set-up.

X-ray scattering measurements have been performed at the Austrian SAXS beamline of ELETTRA synchrotron in Trieste (Italy) described in Figure 2.3.

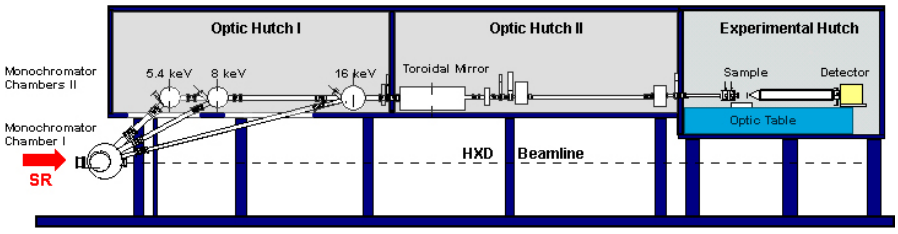

Fig. 2.3: Scheme of the Austrian SAXS beamline at Elettra.

With the same equipment is also possible to record wide-angle X-ray scattering analysis by mean of a second detector set at an opportune angle. This kind of set-up is extremely useful to perform in-situ time-resolved measurements and it has

been used during this work. Performing in situ SAXS measurements during dip-coating is fundamental to obtain a time-resolved sequence of diffraction patterns which informs us on the structural evolution of the structure.

2.2.3 Atomic force microscopy

Scanning probe microscopy (SPM) uses the interaction between a sharp tip and a surface to obtain an image. The sharp tip is kept very close to the surface to be examined and is scanned back-and-forth. For non conductive materials the utilized technique is Atomic Force Microscopy (AFM). It can analyze insulating materials simply because the signal corresponds to the force between the tip and sample, which reflects the topography of the sample surface. The working principle is the measurement of the interactive force between a tip and the sample surface using special probes made by an elastic cantilever with a sharp tip on the end [50]. The force applied to the tip by the surface, results in bending of the cantilever 2.4. There are typically three different modes for AFM topography: contact and semi-contact and non-contact mode. In contact mode, the tip touches the sample but it can lead to sample damage from the dragging tip on soft materials. Tapping (or semi-contact) mode avoids this drawback: the tip is oscillated and only touches intermittently, so that dragging during scanning is minimized. Non-contact mode is where the tip feels only the attractive forces with the surface, and causes no damage. It is technically more difficult to implement since these forces are weak compared with contact forces. In non-contact mode at larger tip-surface separation, the imaging resolution is poor, and the technique not often used. However, at small separation, true atomic resolution can be achieved in non-contact mode AFM.

Measuring the cantilever deflection, it is possible to evaluate the tipŰsurface interactive force. The interactive forces measured by AFM can be qualitatively explained by considering, for example, the van der Waals forces. The van der Waals potential energy of two atoms, located at a distance r from each other, is

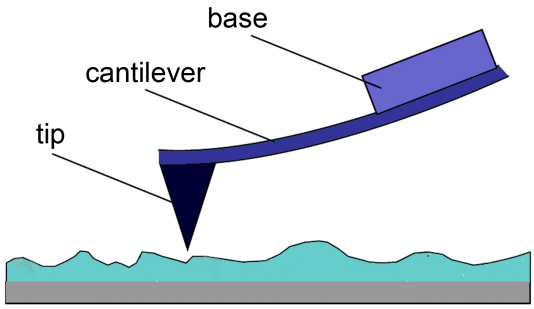

Fig. 2.4: AFM probe schematic drawing.

approximated by the exponential function - Lennard-Jones potential:

$$U_{LD}(r) = U_0 \left\{ -2 \left(\frac{r_0}{r} \right)^6 + \left(\frac{r_0}{r} \right)^{12} \right\} \tag{2.1}$$

The first term of the sum describes the long-distance attraction caused, basically, by a dipole-dipole interaction and the second term takes into account the short range repulsion due to the Pauli exclusion principle. The parameter is the equilibrium distance between atoms, the energy value in the minimum. Lennard-Jones potential allows to estimate the interaction force of a tip with a sample. The energy of the tip-sample system can be derived, adding elementary interactions for all the tip and sample atoms. Acquisition of an AFM surface topography may be done by recording the small deflections of the elastic cantilever. For this purpose optical methods are widely used in atomic force microscopy. The optical system is aligned so that the beam emitted by a diode-laser is focused on the cantilever, and the reflected beam hits the center of a photodetector. Four-section split photodiodes are used as position-sensitive photodetectors.

Atomic force microscopy measurements have been performed by a NT-MDT Ntegra AFM in semi-contact mode.

2.2.4 Transmission electron microscopy

TEM is an efficient and versatile technique for the characterization of materials, it is used to investigate the internal structure of micro- and nanostructures. The

electron microscope is built like a series of vessels connected by pipes and valves separating all the vessels from each other. The vacuum around the specimen is around 10^{-7} Torr. It works by passing electrons through the sample and using magnetic lenses to focus the image of the structure. Because the wavelength of the electrons is much shorter than that of light, much higher spatial resolution is attainable for TEM images than for a light microscope. TEM can reveal the finest details of internal structure, in some cases individual atoms. TEM and high-resolution transmission electron microscopy (HRTEM) are among the most important tools used to image the internal structure of a sample. The uniqueness of TEM is the ability to obtain full morphological properties from the sample. This technique widely used for analyzing porous materials. TEM in mesoporous films can give direct high quality images of the mesostructure. Typically, the film is scratched from its substrate depositing the fragments on a carbon coated grid for observation. Mesoporous films which have undergone full removal of the template generally give better quality images than samples where the organic mesophase is still present within the film: this is because the former has a high electronic contrast between the matrix and the pore (silica-void), whereas the latter provides a lower electronic contrast between the matrix and the pore template.

TEM measurements have been obtain in collaboration with Dr. Maria Francesca Casula at Chemical Department in University of Cagliari through a Transmission Electron Microscope Jeol 200CX equipped with a tungsten cathode operating at 200 kV.

Chapter 3

Results

This chapter describes the most relevant results achieved during this doctorate work. It can be divided in three main subjects, each of them showing an improvement concerning thin porous silica films. Firstly, an implementation of the patterning of mesoporous silica films through deep X-ray lithography has been obtained adding the simultaneous gold nanoparticles growth. For pratical applications, the presence of gold nanoparticles at the interface between a biological analyte and the porous matrix, in fact, should allow a strong increase in the detection signal due to a collective oscillation of conduction electrons of the metal nanoparticles (plasmon). The choice to use the pores as host for biological species makes relevant the need of larger pores so hierarchical porous silica films are described which have been obtained by organic and inorganic templating agents through an EISA process. The importance of such films are represented not only in the hierarchy but mainly in the selective opening of pores which allows separate functions to different pores. Finally a variation in the precursors solution has been done together with an aging process in order to obtain a phase separation in the film giving rise to a homogeneous distribution of pores of similar dimension but different shapes and selectivity. All the achievements are correlated by the leading aim of integrating the films in a device such as lab-on-a-chip.

In all the performed experiments, the oxide component is silica while methiltriethoxysilane (MTES) and tetraethoxysilane (TEOS) have been used as typical precursors. Acid catalyzed conditions have been adopted in all the samples using

hydrochloric acid as typical catalyst.

3.1 Mesopores and nanoparticles

In this section a new step in patterning of mesoporous films is reported. Starting from the DXRL as a patterning technique for mesoporous silica films, we have been able to integrate gold nanoparticles formation with the existing patterning technique in a simultaneous process. Thus giving rise to a patterned thin silica films with gold nanoparticles embedded within the film [48].

Materials

A precursor sol containing the silica source (TEOS and MTES) has been prepared by adding in the following order: ethanol EtOH, TEOS, MTES, and aqueous HCl in the molar ratios Si : EtOH : H_2O : HCl = 1 : 2.78 : 1.04 : 1.4x10^{-2}, where *Si* stands for a mixture of TEOS and MTES whose molar ratio c=[MTES]/[TEOS] has been set to 0.5. This sol (mother solution) has been stirred for one hour at room temperature to prehydrolyze the silicon alkoxides. Another solution (templating solution) has been prepared by dissolving 1.3 g of Pluronic F127 in a mixture of 15 ml EtOH and 1.5 ml acid aqueous solution (5.7x10^{-2} M). The final precursor sol, which has been obtained by adding 7.7 ml of the mother solution to the templating solution, has been left under stirring for further 24 h. Tetrachloroauric(III) acid hydrate, $HAuCl_4$, has been used as gold precursor and dissolved in the TEOS-MTES-surfactant sol until a transparent yellow solution was finally obtained. The final molar ratios were Si : EtOH : H_2O : HCl : F127 : $HAuCl_4$ = 1 : 16.3 : 5.4 : 1.9x10^{-2} : 5x10^{-3} : 3.7x10^{-3}. The silicon substrates have been dip-coated in the precursor sol at 5 mm/s withdrawal rate and 30% relative humidity (RH), the films have been exposed to X-rays immediately after the deposition.

3.1.1 Patterning and gold nanoparticles formation

The as-deposited films have been patterned using the deep X-ray lithography. The samples have been exposed through X-ray masks containing test patterns of different size, shape and geometry from 5 to 500 μm). The masks had a gold absorber 20 μm thick and a titanium transparent membrane 2.2 μm thick. X-ray doses in the 0.8-14 kJ cm^{-3} range have been used for patterning. The etching solution has been prepared with a mixture of ethanol (15 ml), ethylene glycol (30 ml), and water (1 ml). The solution has been optimized to obtain the etching in a time scale of 5 min and the maximum aspect ratio for the patterned structures. The developed films have been rinsed with EtOH and dried under a nitrogen flow.

The overall process is illustrated in Figure 3.1. The mesostructured film, which contains the gold precursor and the templating micelles (Figure 3.1a), is exposed to X-rays through a mask just after the deposition (Figure 3.1b). The effect of X-rays is to remove the template, to condense the inorganic pore walls and finally to promote the formation of gold nanoparticles within the porous matrix of the films as shown in Figure 3.1c. The whole process is explained in details in the following section.

The final processing step is the chemical etching that allows removing the unexposed part of the film (Figure 3.1d). The highly energetic X-rays are used as an efficient writing tool that plays a multiple effect on the mesostructured films. Also, the exposure to an intense X-ray source does not disrupt the mesophase, even after the removal of the surfactant template [2]. By adjusting the dose it is possible to change the X-rays effect on the materials, thus controlling some of the properties.

The high energy X-rays on the material have different effects such as a promotion of a fast and direct formation of gold nanoparticles in the exposed part of the films and the condensation of the pore walls. The effects are simultaneous and clearly the kinetics of the different processes involved must be well balanced to obtain functional materials with tunable properties on a nanoscale. The material mesostructure is not affected by X-rays exposure and subsequent etching; in particular etching, which is generally a very critical step, is easy and fast and is based on the fact that the exposed part of the film is preferentially densified by

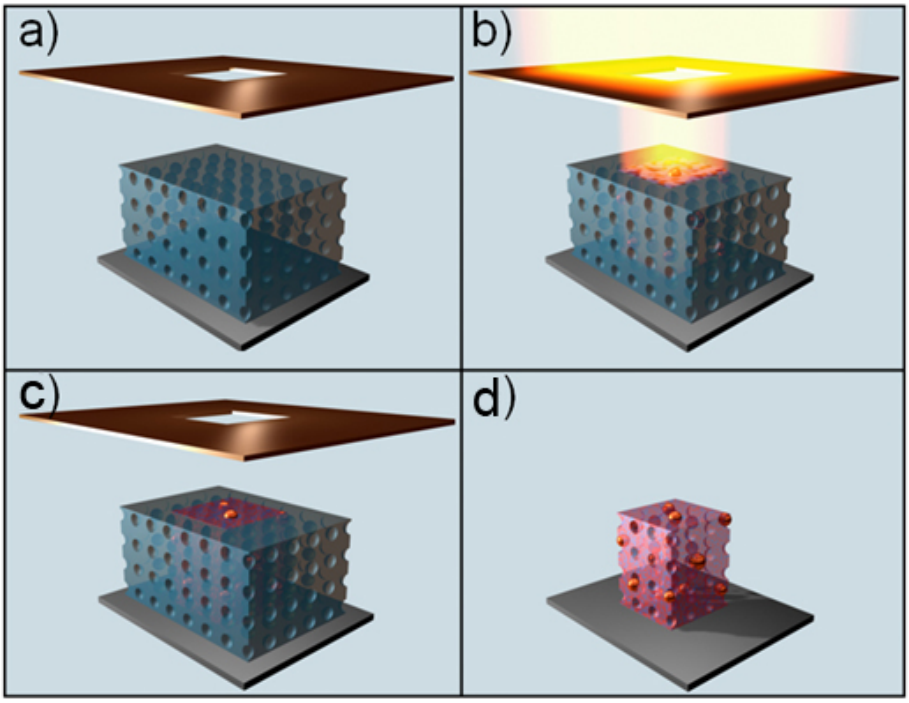

Fig. 3.1: Illustration of the integrated top-down and bottom-up lithographic process. (a) The mesostructured film containing the gold precursor and the templating micelles is (b) exposed just immediately after the deposition to an X-ray beam through a mask. (c) X-rays remove the template, condense the inorganic pore walls, and promote the formation of gold-nanoparticles within the porous organized matrix of the film. (d) Chemical etching allows removing of the unexposed part of the film.

effect of X-rays. Even if the mechanism is not completely clear, supposingly and in according to the literature, the formation of radical species induced by X-rays promotes the densification of silica via silanols condensation reactions. The free radicals, $H^{\cdot}$ and $OH^{\cdot}$, are formed by dissociation of water molecules exposed to ionization radiation [51]. Residual adsorbed water is always present in sol-gel and mesoporous films and is the source of the free radicals. Besides promoting densification of the inorganic walls and depolymerization of the organic template, the same radicals are also responsible for the gold reduction. The hydrogen radicals act as electron donors to reduce the $HAuCl_4$ to metallic gold [52][53] through the reactions :

$$HAuCl_4 \rightarrow H^{\cdot} + AuCl_4^{-}$$

$$H_2O \rightarrow H^{\cdot} + OH^{\cdot}$$

$$4OH^{\cdot} \rightarrow 2H_2O + O_2$$

$$AuCl_4 + 3H^{\cdot} \rightarrow Au + 3H^{+} + 4Cl^{-}$$

A side product of this reaction is HCl, which could have some local densification effect even if its contribution to total condensation of the matrix is negligible. The intensity of the dose is a critical parameter because it controls the degree of condensation of the pore walls and the formation of gold nanoparticles.

Chemical characterization

The exposure of the silica matrix to X-rays produces, as previously said, different and simultaneous effects such as removal of the surfactant, densification of the silica pore walls, partial removal of the methyl groups that are covalently bonded to silicon in the hybrid matrix and formation of gold nanoparticles. The densification process has been analyzed by FTIR spectroscopy. Absorbtion spectra has been recorded at different film conditions in the 1300-850 cm^{-1} range on the hybrid organic-inorganic films before and after exposure to increasing X-ray doses. The spectra are reported in Figure 3.2 showing some distinct absorption bands: one of small intensity which is peaking around 1275 cm^{-1} and is attributed to

Si-CH_3 symmetric deformation [54] a second wide and intense band around 1050 cm^{-1} which is assigned to Si-O-Si antisymmetric stretching, this band is overlapped to another intense band peaking around 1100 cm^{-1} that is assigned to unreacted alkoxy species [55] and the third one around 950 cm^{-1}, which is assigned to Si-OH.

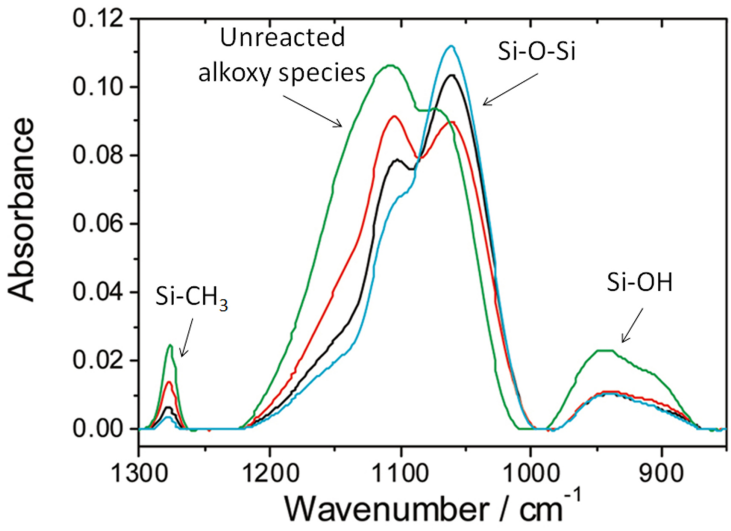

Fig. 3.2: FTIR absorption spectra in the 1300-850 cm^{-1} range of the hybrid films before and after exposure to different X-ray doses: green line, as deposited; red line, 0.6 kJ cm^{-3}; black line, 1.8 kJ cm^{-3}; cyan line, 3kJ cm^{-3}.

The CH_3 and Si-OH bands decrease in intensity with the increase of the X-rays exposure dose and give a direct indication of the effect of synchrotron light on the organic components within the films and on silica condensation.

Infrared imaging has been also used to evaluate the effect of X-rays on the film. Figures 3.3a and 3.3b show the optical image of a patterned and etched film deposited on a silicon substrate and the corresponding infrared image obtained by integrating the absorbance of the Si-O-Si vibrational band in the 1250-980 cm^{-1} range. The image shows that the patterned areas are formed by silica whose signal is not observed in the etched areas, indicating that the chemical etching process is really effective in removing the part of the film that has not

been exposed to X-rays from the substrate.

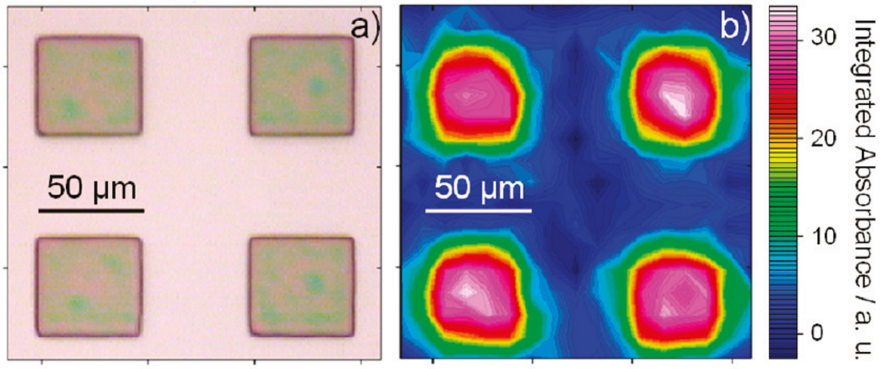

Fig. 3.3: a) Optical image of a patterned and etched film deposited on silicon substrate; b) corresponding infrared image obtained by integrating the absorbance relative to the Si-O-Si band.

Physical characterization

Samples has been also analyzed to obtain morphological and physical informations. Figure 3.4 shows the brightfield TEM images of as-deposited mesostructured films exposed to different X-ray doses: 2.8 kJ cm^{-3} (Figure 3.4a) and 14 kJ cm^{-3} (Figure 3.4b); gold nanoparticles, which appear as dispersed black dots within the silica matrix in the TEM images, are directly formed after exposure to X-rays.

A higher dose promotes the formation of a higher density of gold nanoparticles, which have similar dimensions (within the experimental error) as indicated by TEM images: 5.6 $\pm$1.8 nm at 14 kJ cm^{-3} and 6.5 $\pm$1.8 nm at 2.8 kJ cm^{-3}. The same samples have been treated at 250°C to observe also the mesopores (Figure 3.4 c, d). Thermal treatment is indeed able to increase the electron density contrast allowing the observation of the mesostructure by TEM. As-deposited films have, in fact, a low electron density contrast that does not allow a direct observation of the organized mesostructure; the pore dimensions estimated from the TEM images has been calculated to be 6.7 $\pm$1.8 nm, which is in the same order of magnitude of gold nanoparticles before thermal treatment. After thermal

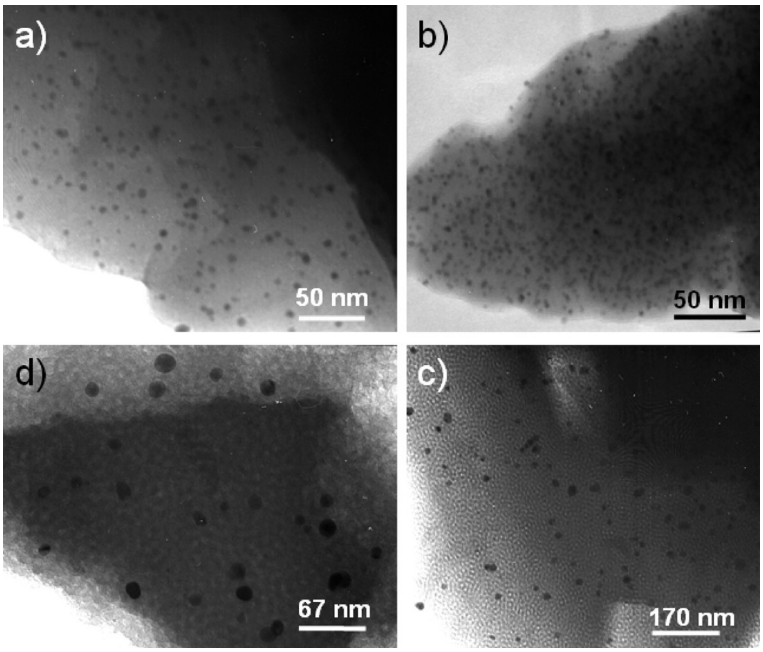

Fig. 3.4: Bright-field TEM images of as deposited mesostructured films exposed to different X-ray doses: (a) 2.8 and (b) 14 kJ cm^{-3} doses. (c, d) same samples after thermal treatment to 250°C.

treatment the gold nanoparticles grow and assume a broader size distribution. Particle size distribution shown in Figure 3.5 has been estimated from the bright field TEM measurements in Figure 3.4 using a specific routine running on IgorPro software.

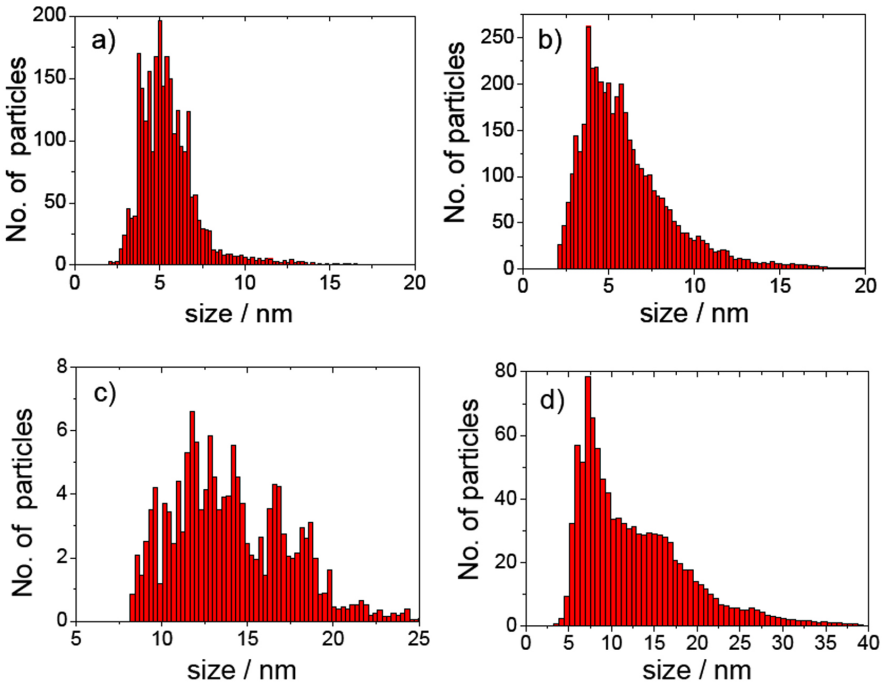

Fig. 3.5: Nanoparticle size estimation and distribution obtained from TEM images of as deposited mesostructured films exposed to different X-ray doses: 2.8 kJ cm^{-3} (a) and 14 kJ cm^{-3} doses. The same samples after thermal treatment at 250°C (c and d).

The deep X-rays lithographic process produces well defined patterns even in the case of complex shapes as shown in the optical images of Figure 3.6 a, b and c. The pictures show some examples of different patterns. The optical images are taken from as deposited films on silicon after exposure to X-rays and before etching. The pink-red color is indicative of the presence of gold nanoparticles, while the unexposed part of the film appears light blue. The same pattern of Figure 3.6c after etching is shown in the SEM image in Figure 3.6d; the pattern appears highly regular with a good aspect-ratio.

The quality of the process, which allows obtaining defined patterns and meso-

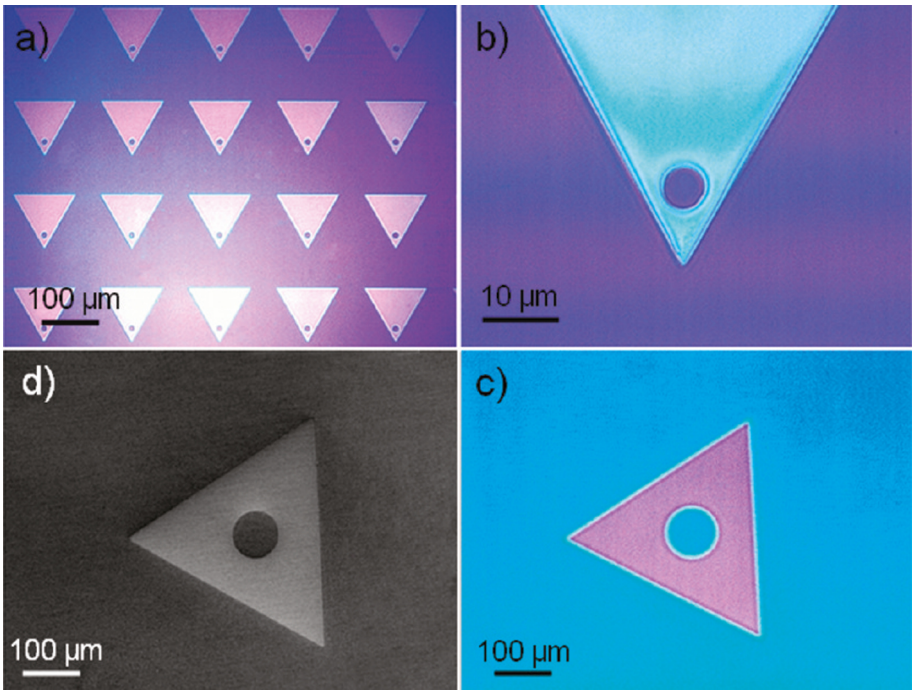

Fig. 3.6: Optical images taken from as deposited films on silicon after exposition to X-rays and before etching. The pink-red color is indicative of the presence of gold nanoparticles, whereas the unexposed part of the film appears light blue. The same pattern of image c after etching is shown in the SEM image in d.

porous arrays doped with gold nanoparticles, is clearly demonstrated by Energy Dispersion X-ray Spectroscopy (EDS) analysis of a patterned film in Figure 3.7. The images show the SEM image of a patterned microstructure on silicon substrate after etching (Figure 3.7a) and the EDS images obtained by measuring the signals of gold (Figure 3.7b) and silicon (Figure 3.7c).

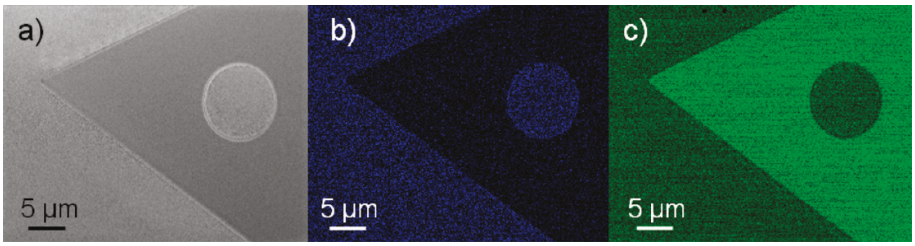

Fig. 3.7: SEMimage of a patterned microstructure on silicon substrate after etching (a) and the EDS images obtained by measuring the signals of gold (b) and silicon (c). A darker color is correlated with a lower signal intensity.

A darker color is correlated with a lower signal intensity. The Au signal is observed in the developed part of the film, whereas the Si signal, which is given by the silicon substrate, is more intense in the etched one. The EDS signal of gold appears homogeneous and indicates that gold nanoparticles are well dispersed and distributed in the sample. The optical images of a gold-doped patterned mesostructure deposited on glass slide after etching in Figure 3.8 show that the final material is highly defined and homogeneous. The quality of the process, which includes the chemical etching, has been evaluated by AFM analysis.

Figure 3.9 shows the AFM images on 80x80 and 50x50 μm^2 areas of a patterned sample on silicon substrate. The developed microstructures show a height of ∼600 nm with a sharp profile; the possibility to pattern films thicker than 0.5 μm is a clear advantage of deep X-ray lithography. It is, in fact, possible to fabricate complex patterns with a sharp profile and a high aspect ratio. The high energy of the X-rays allows achieving a homogeneous and deep lithography even in very thick films, which is not possible to obtain with other common techniques such as soft X-rays or UV light.

UV-visible absorption spectrum and and X-ray diffraction pattern of a mesostructured film deposited on cover-glass slide and exposed to 14 kJ cm^{-3} X-ray

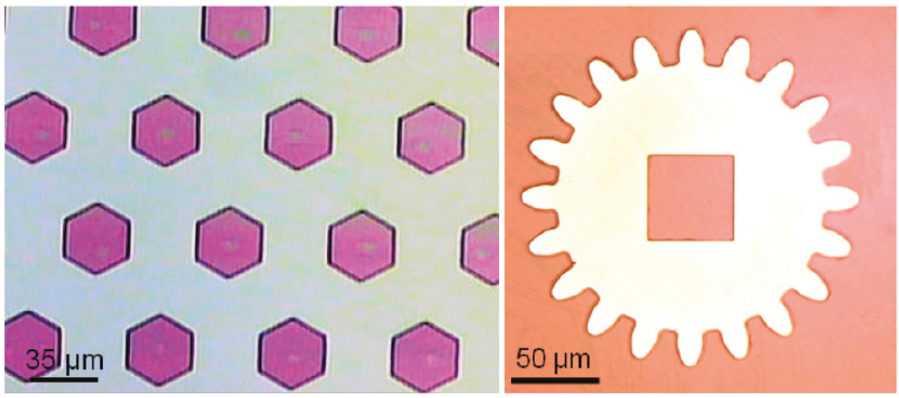

Fig. 3.8: Optical images of a gold-doped patterned mesostructures deposited on glass slide after etching.

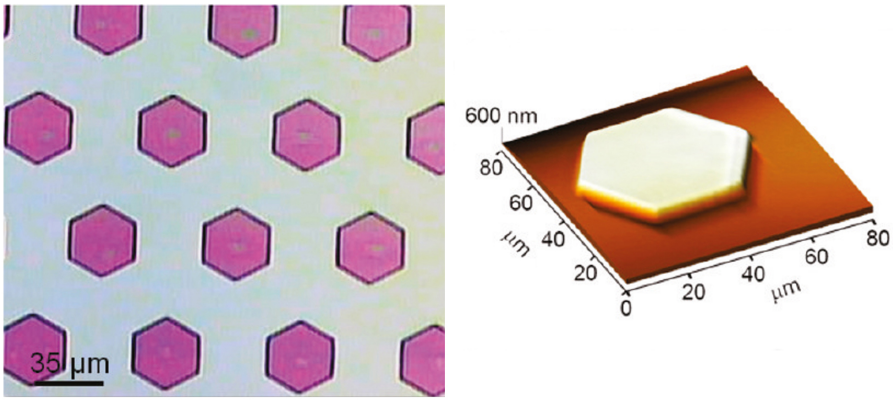

Fig. 3.9: AFM images on 80x80 μm^2 area of a the patterned sample on silicon substrate and relative optical image.

dose are shown in Figure 3.10.

The UV-vis spectrum shows an absorption band peaking at 534 nm and the X-ray diffraction pattern shows the fingerprints of metallic gold. Both measurements confirm the formation of gold nanoparticles upon X-ray exposure. We have evaluated the size of gold nanoparticles from the plasmonic peak of UV-vis spectra [56]. The particles, from TEM images, can be described as spherical in good approximation so we have calculated that the average dimension is 5.6 nm, whereas the nanoparticle size is 9.6 $\pm$3 nm when the Scherrer equation is applied to the X-ray patterns. Both the values are in good agreement with the nanoparticles size measured by electron microscopy.

A qualitative measurement of the SERS signal has been done in X-Ray exposed films in the presence of gold nanoparticles. Figure 3.11 shows the rhodamine 6G Raman signal in an exposed and not-exposed region of the silica film.

The measurement shows a strong increase in the Rh6G detected signal in the sample containing gold nanoparticles thus confirming the expected effect [57].

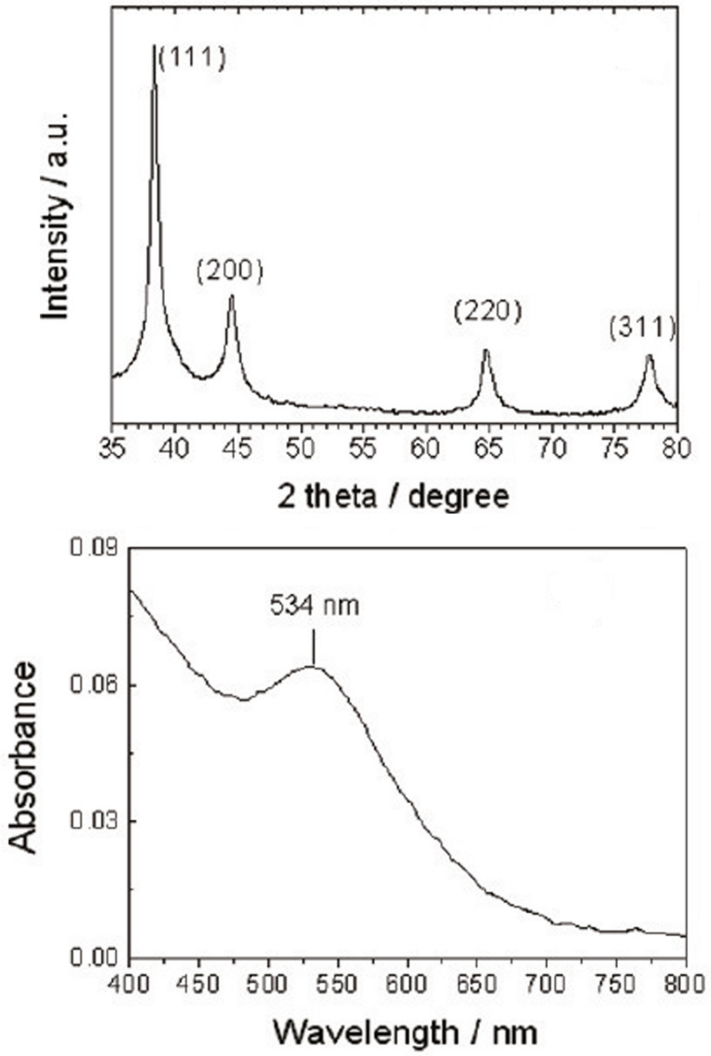

Fig. 3.10: X-ray diffraction pattern and typical UV-vis absorption spectrum of a mesostructured film deposited on cover-glass slide and exposed to a 14 kJ cm^{-3} X-ray dose.

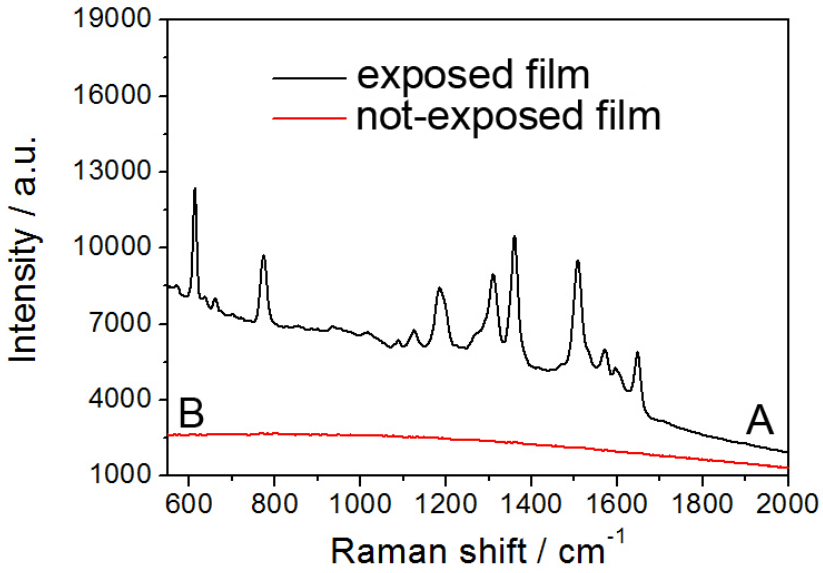

Fig. 3.11: SERS spectra of Rh6G for the silica film with gold nanoparticles. Spectrum A is recorded in the X-ray exposed film, spectrum B is recorded in the unexposed region of the film. Spectra A and B were recorded under identical experimental conditions with a laser excitation of 633 nm.

3.2 Hierarchical thin films

In this section an alternative route to hierarchical porous films through evaporation-induced self-assembly (EISA) is described [58]. We have created a two-order of pores material by a one-pot templating method. Mesopores are produced by the usual surfactant self-assembly while the choice of the second template is dictated by the limitation that it should not interfere with the self-assembly process and should allow a pore dimension and shape control, if possible. Finally it should be easily removable avoiding the damage of the mesoporous matrix.

3.2.1 Mesopores and nanoboxes

The process is based on forming a second template nanostructure during EISA that can be easily and selectively removed at the end of film processing. The idea is to nucleate inorganic nanocrystals within the film which can be easily removed, in that direction, NaCl crystals appear optimum to this aim. The formation of salt nanocrystals acting as templating agent for pores can be naturally driven by evaporation of the solvent leading to a general synthesis method for producing pores of well defined shapes and hierarchical porous thin films.

Materials

The precursor solution has been prepared using a triblock copolymer surfactant, Pluronic F127, TEOS, MTES, EtOH, sodium chloride, (NaCl), and sodium phosphate monoacid, (Na_2HPO_4). This solution has been prepared in different steps: at first we have prepared a sol, following a well established protocol previously optimized [59], for the preparation of MTES-TEOS hybrid organic-inorganic mesoporous films. This protocol allows preparing hybrid organic-inorganic films that exhibit a strong capability to form highly organized mesostructures using block copolymer surfactants. We have used a triblock copolymer (F127) as template which is easily removed upon calcination of the film in air at temperatures between 150 and 350°C [60]. This temperature is low enough to maintain the covalently bonded methyl groups into the film without affecting the organization

of the mesophase. The presence of the methyl groups is very important because they limit the absorption of water into the mesopores [61].

The sol has been obtained in two stages; in the first one a stock solution has been prepared by mixing 3.08 ml of EtOH, 2.84 ml of TEOS, 1.42 ml of MTES, and 0.355 ml of an acidic water solution (HCl $7.68x10^{-1}$M); the solution has been stirred for 1 h at 25°C in a closed vessel. In the second stage a solution containing the surfactant has been prepared by dissolving 1.3 g of Pluronic F127 in 15 ml of EtOH and 1.5 ml of acidic water (HCl $5x10^{-3}$M). Finally the two solutions have been mixed together and stirred for 15 min at 25°C in a closed vessel. The final molar ratios of the mixture are the following: TEOS : MTES : EtOH : H_2O : HCl : F127 = 1 : 0.56 : 24.48 : 8.13 : 0.11 : $7.6x10^{-3}$. Then we have prepared a salt solution by dissolving NaCl and Na_2HPO_4 in water at different relative concentrations as reported in table 3.1 and we have added this salt solution to the silica sol.

NaCl	Na_2HPO_4
0.49 M	32 mM
0.7 M	45.5 mM
0.84 M	54 mM

Tab. 3.1: Concentration of NaCl and Na_2HPO_4 in water generating nanocubes.

In a typical preparation 20 ml of the MTES-TEOS-Pluronic solution are added to 3.6 ml of mixed salt aqueous solution. After the addition of the aqueous salt solution of NaCl and Na_2HPO_4, the MTES-TEOS sol becomes quickly transparent and the films appear optically homogeneous and transparent.

The work has been performed in a systematic way, for this reason a sol containing only NaCl or Na_2HPO_4 using the same recipe and molar ratios has been prepared in order to compare the effects induced by the salt solution. Film have been deposited on silicon substrates, previously cleaned with water and EtOH, by dip-coating deposition at a 15 cm/min withdrawal rate. The temperature in the deposition room has been kept at 25°C and the relative humidity (RH) at 25%. The films, immediately after their deposition, have been dried at 80°C for 18 hours in air, then at 150°C for 2 hours, and finally calcined in air at room

pressure at 350°C for 3 hours.

Chemical characterization

A complete characterization of the films has been performed. X-ray diffraction (XRD) patterns have been recorded and far-infrared spectroscopy (FIR) measurements have been acquired in order to identify the nanocrystalline templating phase that has formed by EISA. Measurements of sample 0.7 M NaCl-45.5 mM Na_2HPO_4 are shown in Fig.3.12 and Fig. 3.13, both the data show that it is crystalline sodium chloride. X-ray diffraction measurements were recorded in an $\omega/2\theta$ scan from 25° to 60° with a step of 0.02°. The XRD pattern in the 25-60° range shows four sharp diffraction peaks, 111, 200, 220, and 222, which represent the typical fingerprint of crystalline sodium chloride; the XRD patterns of the sample without the salt and after washing show only the background noise.

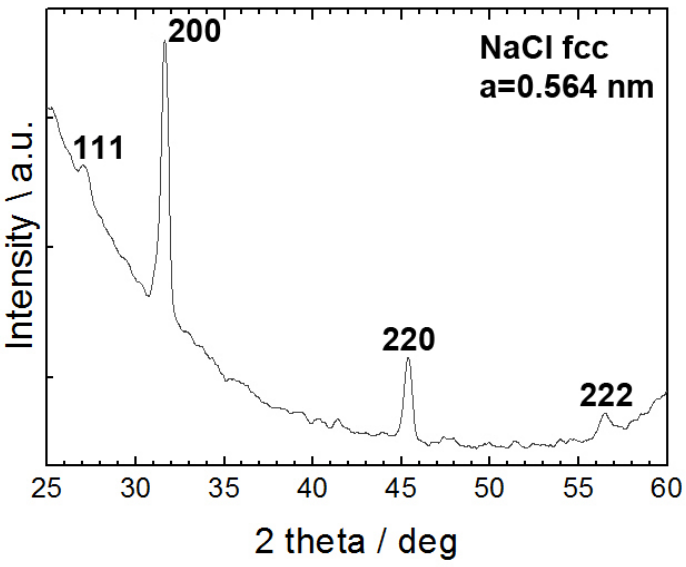

Fig. 3.12: XRD pattern of a mesoporous film containing the salt nanocrystals; the indexation of the crystalline phase is shown (sample 0.7 M NaCl-45.5 mM Na_2HPO_4).

Fourier transform infrared (FTIR) analysis has been performed using a Bruker Vertex 70 V spectrophotometer. The optical bench and the sample compartment

have been kept in a vacuum during the measurement at a pressure lower than 0.5 hPa. The measurements have been done using a Globar source, a Si beamsplitter, and a RT-DTGS-FIR detector. The spectra have been recorded in transmission, in the 600-50 cm^{-1} range by averaging 32 scans with 4 cm^{-1} of resolution. A silicon wafer has been used as the substrate to measure the background; the baseline has been calculated by a rubberband algorithm (OPUS 7 software) while no smoothing on the data was performed.

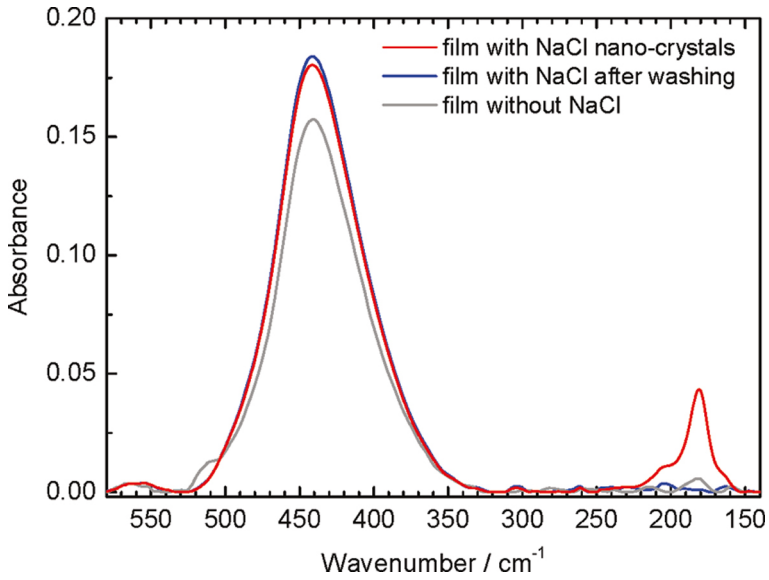

Fig. 3.13: Far-infrared spectrum in the 580-140 cm^{-1} range of films at different steps of preparation (sample 0.7 M NaCl-45.5 mM Na_2HPO_4).

The Far-IR spectra show an intense absorption band at 440 cm^{-1} which is assigned to the silica rocking mode and another band at 170 cm^{-1} due to phononic modes in crystalline NaCl. The spectra show that the washing process completely removes the salt within the film and is able, therefore, to leave empty nanoboxes.

Physical characterization

Sample morphology has been analyzed by transmission electron microscopy. Finely ground films scratched from the silicon substrate have been deposited on a carbon-coated copper grid for TEM observations. The images taken by transmis-

sion electron microscopy (sample 0.7 M NaCl-45.5 mM Na_2HPO_4) have revealed the presence of different types of nanoscale structures that appear spherical and cubic (Fig. 3.14). The thermal calcination has removed the templating organic micelles formed by the block-copolymer leaving a porous organized structure with mesopores of spherical appearance and dimensions of 6.3 ± 0.6 nm; they are well organized into a cubic structure by EISA during film deposition.

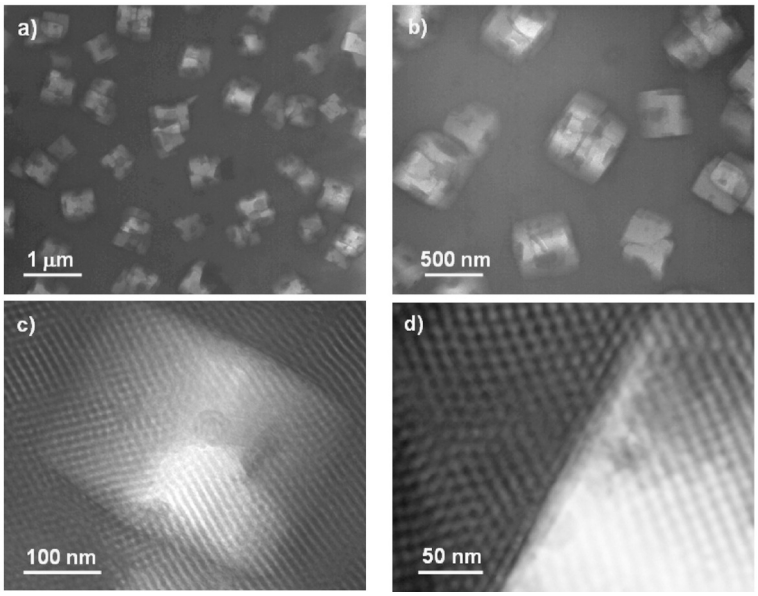

Fig. 3.14: TEM images (a-d) at different magnifications of the film (sample 0.7 M NaCl-45.5 mM Na_2HPO_4) showing the presence of mesopores and nanoboxes.

At the same time the salts added in the precursor solutions have allowed forming another type of nanostructure which appears as cubic boxes of larger dimensions, typically in the range of 100-280 nm. The cubic salt crystals are water-soluble so they can be easily removed by washing the film in water. After removal they leave empty pores. It is important to notice that the overall process does not disrupt the mesophase: the ordered porous phase maintains its arrangement after thermal treatment at 350°C and the following washing process. The typical film thickness after the thermal treatment, evaluated by spectroscopic ellipsometry, is around 400 nm. The evaporation of the ethanol and water during EISA drives self-organization of the templating micelles and also induces precip-

itation of cubic salt nanocrystals as explained in details in the following section by in-situ SAXS-WAXS measurements.

It is meaningful to notice that we have been not able to obtain nanoboxes using only NaCl or Na_2HPO_4 as templating agent, even by a systematic changing in the composition of the sol and the salt concentration. The role of Na_2HPO_4 appears critical in avoiding the precipitation of NaCl and seeding the crystal formation. On the other hand the crystallized salt shows a well-defined shape and dimension which is an indication that the overall process is controlled. Only some specific compositions allow forming NaCl nanocrystals (see Tab.3.2), while in one case (sample 0.7 M NaCl-54 mM Na_2HPO_4) a very peculiar *flake-like* nanostructure is observed. In other samples the formation of white salt precipitates on the film surface is observed (samples 0.84 M NaCl-32 mM Na_2HPO_4 and 0.84 M NaCl-45.5 mM Na_2HPO_4). TEM images of the films containing the salt nanocrystals are shown in Figure 3.15.

	Na_2HPO_4		
NaCl	32 mM	45.5 mM	54 mM
0.49 M	mesopores	mesopores	mesopores
0.7 M	mesopores	mesopores + nanoboxes	mesopores + nanoflakes
0.84 M	mesopores and salt precipitates on film surface	mesopores and salt precipitates on film surface	mesopores + nanoboxes

Tab. 3.2: Summary of the films prepared with the different salt concentrations and the observed phases.

The images of the 0.7 M NaCl-54 mM Na_2HPO_4 film show the presence of piled symmetrical salt nanoboxes of around 100 nm which form a structure that we have called *flake-like* (Figure 3.15 a,b). The AFM film images of the surface (Figure 3.16 a,b) reveal that this peculiar structure forms a very specific pattern also on the surface, where *flower-like* nanostructures, which are due to the piled nanoboxes within the film, are observed.

On the other hand, beside this particular pattern the film surface shows a homogeneous distribution of nanograins that we correlate to the formation of

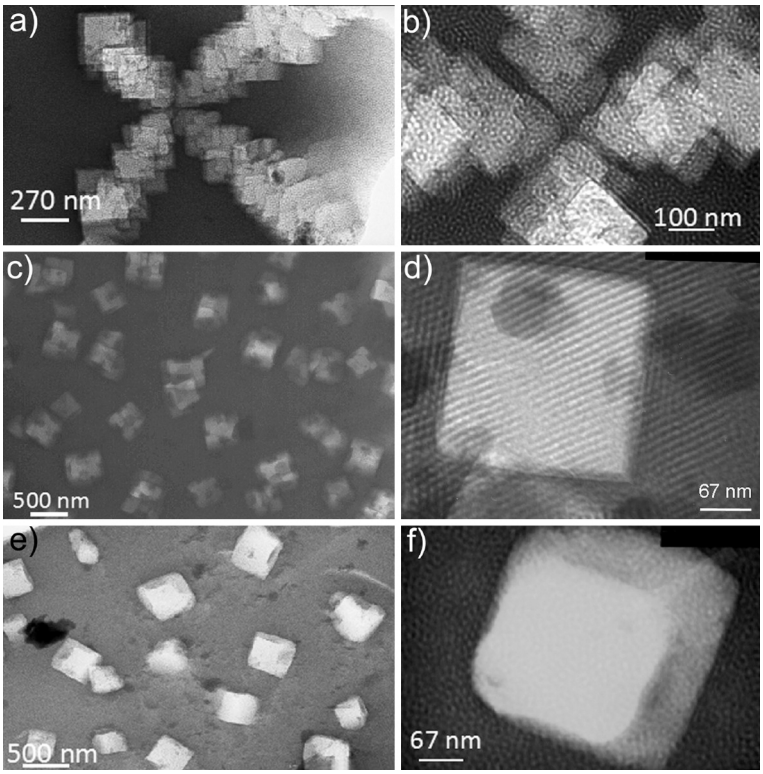

Fig. 3.15: TEM images (a-f) at different magnifications of the films: (a, b) sample 0.7 M NaCl-54 mM Na_2HPO_4; (c, d) sample 0.7 M NaCl-45.5 mM Na_2HPO_4; (e, f) sample 0.84 M NaCl-54 mM Na_2HPO_4.

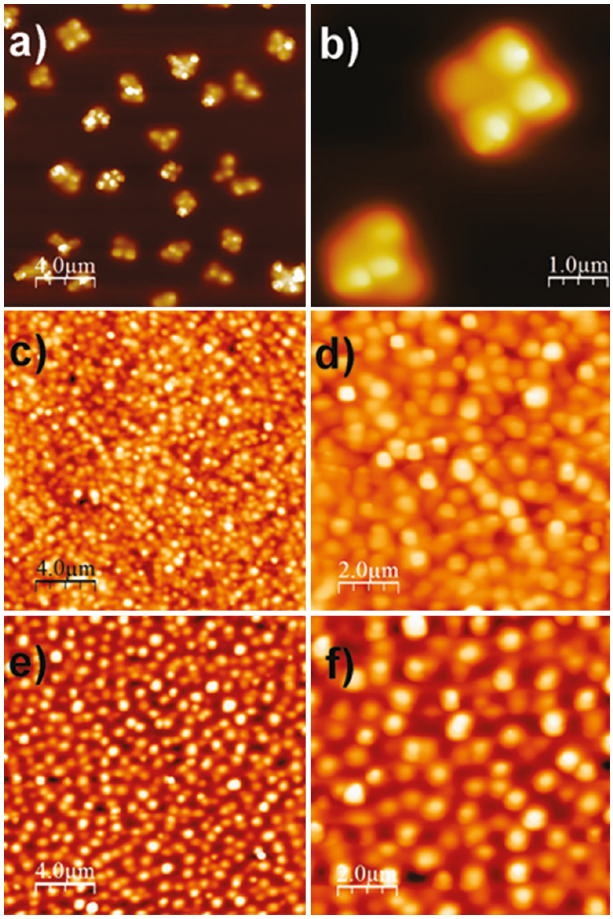

Fig. 3.16: AFM images (a-f) at different magnifications of the films: (a, b) sample 0.7 M NaCl-54 mM Na_2HPO_4; (c, d) sample 0.7 M NaCl-45.5 mM Na_2HPO_4; (e, f) sample 0.84 M NaCl-54 mM Na_2HPO_4.

the salt nanoboxes within the films. It is important to observe that the film homogeneously covers these structures that do not form, even after salt washing out, on the film surface. Figure 3.15 c-f shows the TEM images of the films 0.7 M NaCl-45.5 mM Na_2HPO_4 and 0.84 M NaCl-54 mM Na_2HPO_4; the surface of these films is shown in Figure 3.16 c-f. The nanoboxes formed in the 0.7 M NaCl-45.5 mM Na_2HPO_4 film are bigger with respect to the sample prepared at a lower salt concentration. This process appears simple and highly reproducible; preparation has been repeated several times, always obtaining similar results.

The formation of salt nanocrystals gives pores of well defined shape, while a certain control of pore dimension and topological distribution can be achieved by changing the salt concentration and relative salts composition. The production process of the hierarchical material is illustrated in Figure 3.17: in the first step a mesostructured film is produced by EISA and the film contains mesopores and salt nanoboxes; in the second step the film is calcined in air at 350°C to remove the block copolymer template, the mesopores are now empty, and the nanoboxes are still filled. In the final step the film is washed by water and then dried; this process allows eliminating the salt, leaving empty nanoboxes.

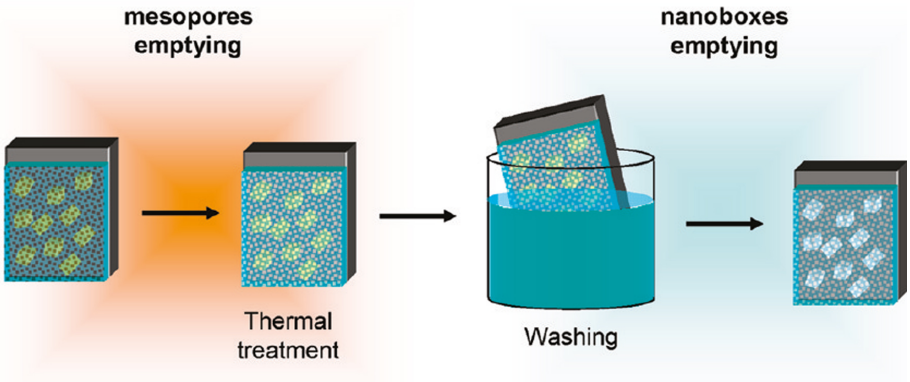

Fig. 3.17: Illustration of the different steps to prepare hierarchical porous films with mesopores (2-10 nm) and cubic pores (50-400 nm).

The presence of Na_2HPO_4 in the solution appears to be fundamental for the nucleation of cubes in the film during deposition. The presence of only NaCl does not allow the formation of cubes. The advantage of this procedure is given by the

selective control of nanopore formation through film processing and that the templates, which are organic micelles and salt nanocrystals, are formed in their final shape during EISA. The nanoboxes are not ordered but result as homogeneously dispersed within the mesoporous matrix.

3.2.2 Simultaneous in-situ time-resolved SAXS-WAXS analysis

We have tried to get a direct understanding of the phenomenon of nanocubic salt formation during the film deposition by an in-situ time-resolved experiment [62]. This experiment combines different analytical techniques, grazing incidence small angle X-ray scattering (GISAXS) and wide angle X-ray scattering (WAXS). In this way we have been able to follow in situ the two simultaneous self-assembly phenomena: the self-assembly of the micelles and the salt crystallization. We used a special experimental setup employing synchrotron radiation as light source for performing the experiments. Measurements have been recorded at the Austrian-SAXS beamline of the ELETTRA sinchrotron facility in Trieste. The experimental set-up is shown schematically in Figure 3.18. In-situ SAXS and WAXS measurements have been performed in 0.7 M NaCl-45.5 mM Na_2HPO_4 which shows a more regular and homogeneous nanocrystals distribution.

The silicon substrate has been placed on a fixed sample holder, while a beaker containing the silica precursor and the salt solution has been brought down vertically after the substrate immersion using a remote-controlled linear module. The X-ray beam hit the as-deposited sample kept at a fixed position and orientation with respect to the X-ray beam.

GISAXS and WAXS measurements were performed by using an incident wavelength of 1.54 A (8 KeV); the angle of incidence was set slightly above the typical critical angle of silica films (0.15°). Two PSD detector have been used to collect simultaneously the Bragg-diffraction peaks from the mesostructure and from the NaCl nanocrystals.

The experiments has been performed by recording a snapshot each second of both the SAXS and WAXS signal of the film up to 512 s from the deposition.

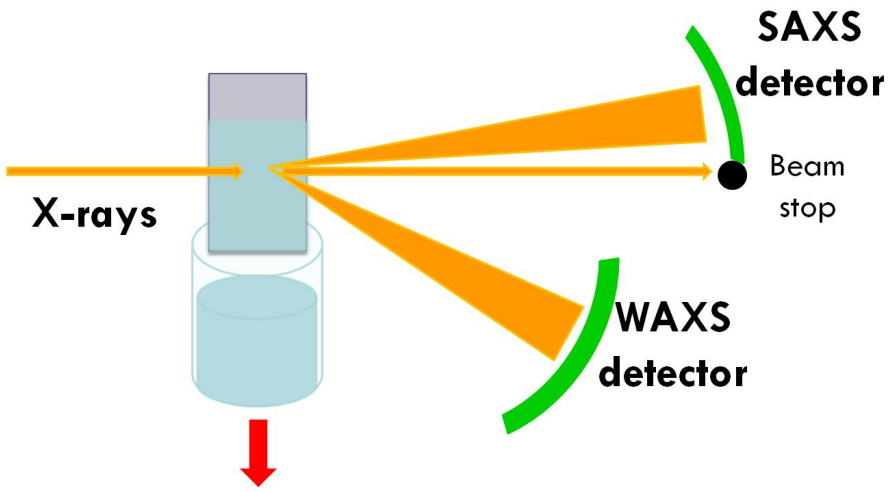

Fig. 3.18: .

The two measurements had the same trigger and therefore can be compared on the same time scale. Figure 3.19 shows the mesostructure peak in time-resolved GISAXS pattern.

The time-resolved WAXS pattern is shown in Figure 3.20 in which the most intense NaCl diffraction peak is clearly visible at 31.8°.

The two different phenomena are both driven by the evaporation of the solvent just after the thin film deposition. The first process is the self-assembly of micelles into an ordered mesostructure and the second one is the nucleation and growth of salt nanocrystals. The SAXS signal is generated by the electronic contrast between the micelles and the silica pore walls while the WAXS signal is due to classic Bragg diffraction of atomic planes in crystalline structures, in particular the 200 fcc NaCl reflection.

The first step of EISA process is characterized by the evaporation of the solvent, in this case ethanol, which produces a strong diffuse scattering at low S_z values; this first initial evaporation stage generally lasts few tens of seconds. At this stage the micelles are not yet formed so there is no signal at higher scattering vector. After around 70 seconds, the rise of an intense signal at 0.077 nm^{-1} is observed, which is attributed to the organization of the micelles into a long range periodic mesostructure and it corresponds to a d-spacing of 12.9 nm.

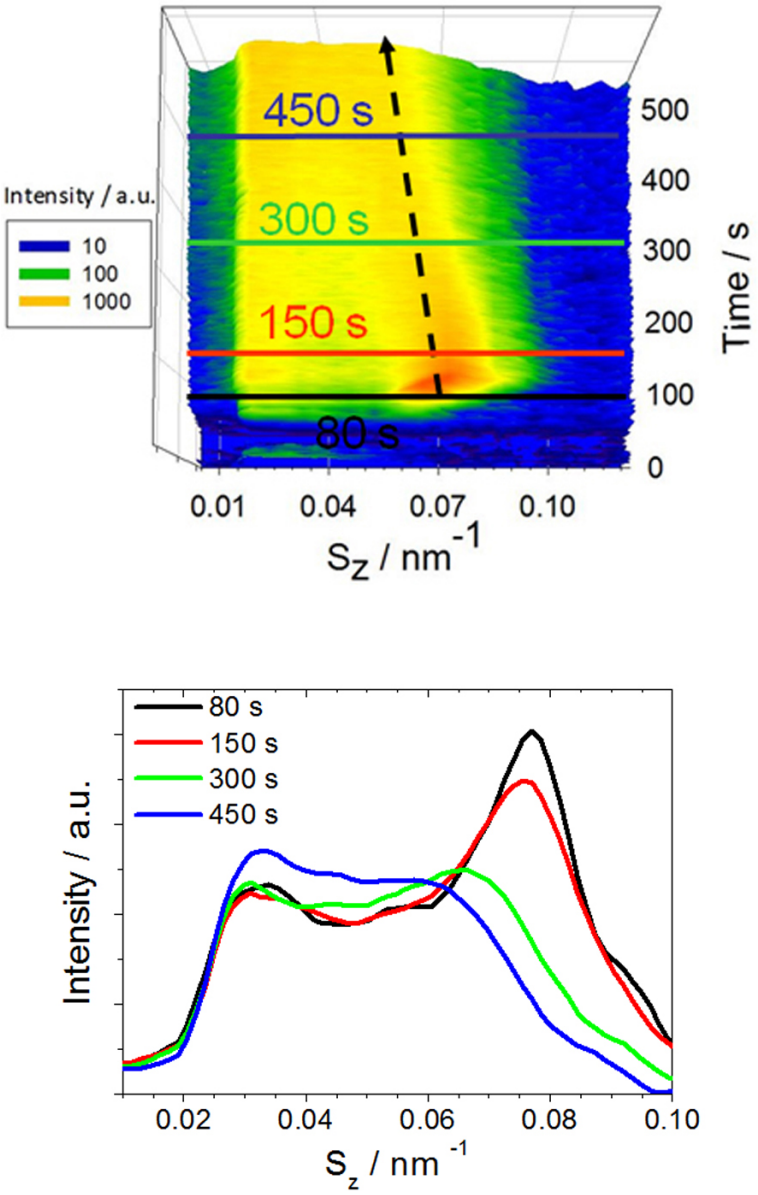

Fig. 3.19: 3D representation of GISAXS time-resolved pattern on hierarchical porous film as a function of time and scattering vector, Sz (top). The intensity variation of the peaks is reported in false colour scale. At the bottom, in situ GISAXS spectra collected after 80, 150, 300 and 450 s from the film deposition.

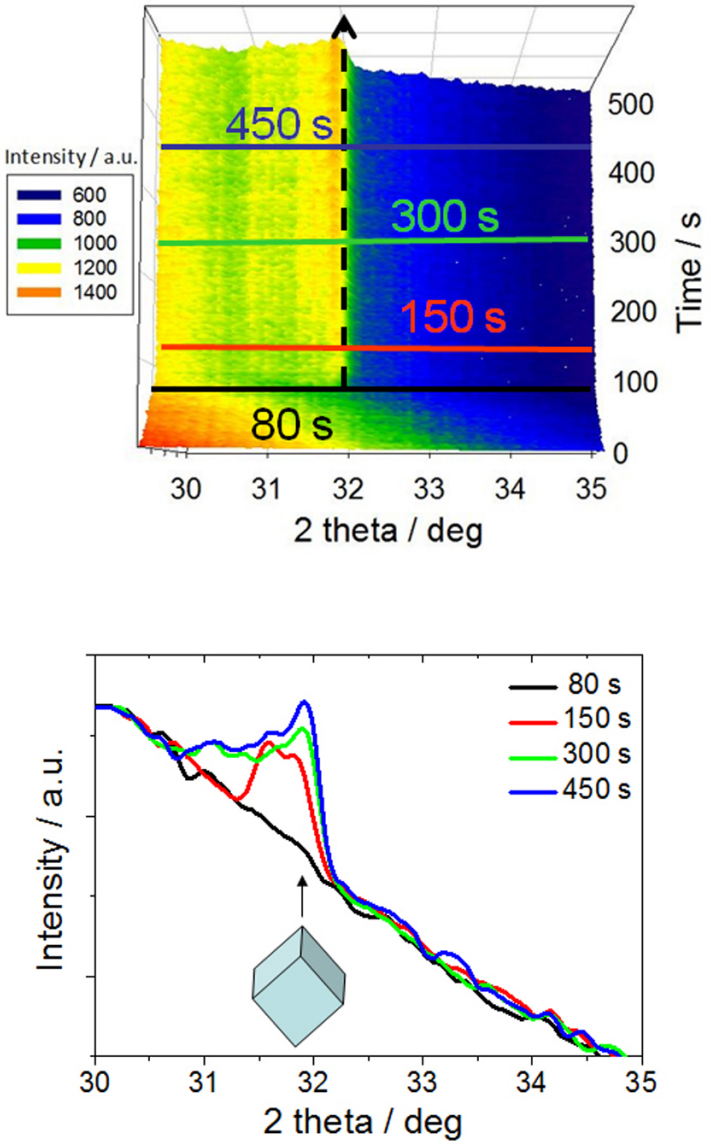

Fig. 3.20: 3D representation of WAXS time-resolved measures on hierarchical porous films as a function of time and 2θ values. The intensity variation of the peaks is reported in false color scale. At the bottom, in situ WAXS spectra collected after 80, 150, 300 and 450 seconds from the film deposition. The peak is attributed to NaCl nucleation and growth.

The maximum intensity of this signal is reached at 80 s from the beginning of EISA process, after this time the signal decreases in intensity and shifts to lower Sz values. The Figure 3.19 and 3.20 show in the bottom the GISAXS pattern after 80, 150, 300 and 450 s and the WAXS pattern at the same times which well describe the overall trend.

Also in WAXS pattern is easy to notice that the first stage of the evaporation process produces a diffuse scattered broad signal. The subsequent crystallization of NaCl is revealed by the rise of a diffraction peak at 31.8° after around 150 s from the beginning of the process. In Figure 3.21 the normalized integrated intensity of the GISAXS and WAXS signals at 0.077 nm^{-1} and 31.8° respectively is shown as a function of processing time; this analysis allows a direct comparison between the two processes: micelles organization and crystal nucleation and growth. The GISAXS curve shows a fast decrease in intensity of the signal which is time-correlated with the simultaneous increase of the WAXS peak. The comparison of the two curves indicates also that there is a small time shift between the two phenomena; the salt crystals appears after 80 s when the micelles are already well formed. In correspondence of the rise of the NaCl diffraction peak, the GISAXS signal on the contrary begins to decrease. Our explanation is that the salt crystals produce a change in the modulation of the electronic density contrast which is at the ground of GISAXS detection of micelles organization. This means that once the crystals are formed, the signals from the micelles can not be directly correlated, in terms of intensity, to their degree of organization.

To obtain a direct proof of the not damaging of mesosctructure even in the presence of a decreasing signal in the GISAXS pattern, a 2D SAXS analysis has been performed on the same sample after thermal treatment at 350°. The films, previously measured by time-resolved experiments, has been calcined at 350°C for 30 minutes immediately after in-situ measurements . Each measure is the average of 10 acquisitions with 2 seconds of integration time. The observed diffraction spots have been attributed to the formation of an organized cubic mesophase. The pattern has been fitted by the Nanocell code [63] and on the basis of this attribution the structure has been assigned to a cubic symmetry mesostructure (Im-3m space group) with the (110) plane oriented perpendicular to the substrate

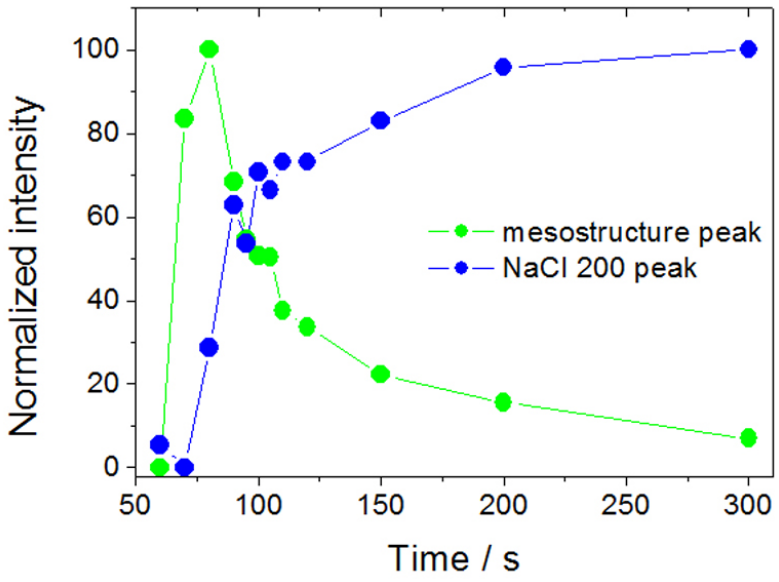

Fig. 3.21: Integrated intensity of the GISAXS (green line) and WAXS (blue line) signals at 0.077 nm-1 and 31.8° respectively as a function of time during simultaneous and time-resolved in situ measures on hierarchical porous films.

(z direction), uniaxially distorted [64]. Following this attribution, the interplanar distances have been calculated (see Fig. 3.22) as d_{110} = (10.3±1.4) nm, d_{101} = (12.3±0.7) nm, d_{-110} = (13.4±0.8) nm. Clearly the addition of the salts into the precursor sol does not interfere with the EISA process during the film deposition.

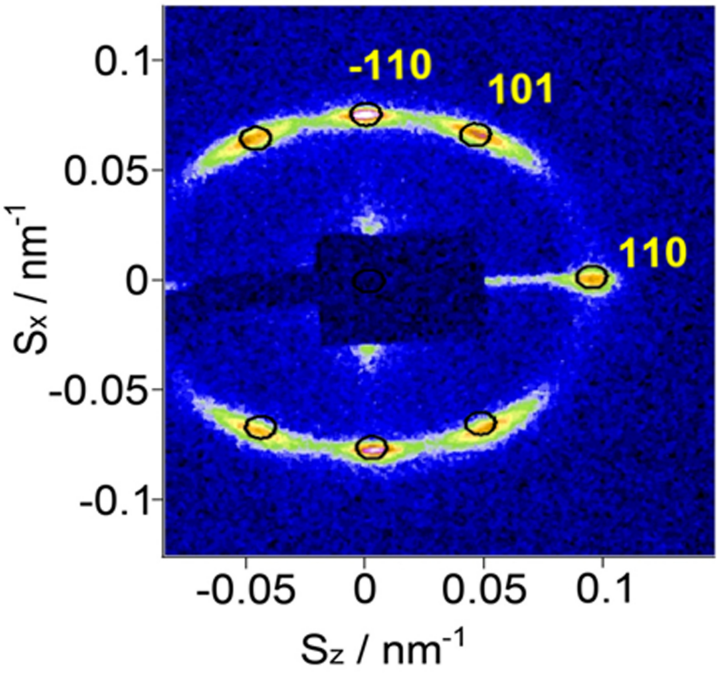

Fig. 3.22: GISAXS pattern of a hierarchical porous films film after thermal treatment at 350° for 30 minutes. Indexation of the body centered cubic organized porous structure is shown.

The data set has shown that the formation of spherical micelles and sodium chloride crystalline templates is a time dependent phenomenon which is simultaneously realized during evaporation. It has to be underlined that the solvent evaporation is a quite complex phenomenon because the presence of a water-ethanol mixture implies different stages of evaporation. Ethanol evaporates faster than water and leaves behind a water enriched phase. Micelles organize at the end of the ethanol evaporation, at this point, in fact, the first SAXS spots are formed. On the other hand the solubility of NaCl is different in ethanol or water rich mixtures; sodium chloride in ethanol at 25°C has a solubility which 481 times

lower than in water [65]. After the full evaporation of ethanol, a water rich film remains and the salt nucleation and growth begins. The growth of the crystals is fast so it is not affected by the proceeding of the polycondensation reactions of the silica network. This mechanism of formation of the two different templates explains the time shift between the rise of the SAXS and WAXS signals.

3.3 Selective macroporous materials

In the alkoxy-derived sol-gel system, various macroporous morphologies can be obtained by inducing the phase separation during the sol-gel transition. This principle of macroporous morphology control can be best applied to pure silica and silica-based multicomponent oxide systems. In this section a procedure to obtain large nanopores of different shapes and dimensions in a silica matrix by mean of phase separation is reported. A similar phenomenon has been well described by Nakanishi et al. [30] for sol-gel powders and monoliths. In this section a reproduction of the phenomenon is reported in thin films, where the phase separation appears a tricky process to control. Potential application of these films are on size- and shape-selective separations, adsorption, and immobilization of proteins and other biological molecules. Silica/surfactant self-assembly allows precise control of the pore size which can be used for controlled release architectures based on incorporation of the release agent in nanoporous hosts.

3.3.1 Aging and phase separation

A step forward to obtain a complex macroporous thin film is represented by the obtaining of porous organic-inorganic hybrid films with well defined pore shape and dimension via a salt-template route and a phase separation process. This achievement is reported in this section. The salt (sodium chloride) precipitates during film deposition as templating for cubic shape pores as already explained in section 3.2.1. Combining this salt-template route with controlled phase separation, is possible to obtain pores of spherical shape within the same film. The dimensions of the nanocubes and nanospheres are in the 20-200 nm range and can be modulated through the film processing conditions. The effect of precursor

solution aging and surfactant concentration on the porous film structure has been sistematicaly investigated using infrared spectroscopy, spectroscopic ellipsometry, X-ray diffraction, Raman imaging, atomic force microscopy and transmission electron microscopy. Results show that only a very specific combination of different synthesis parameters, such as surfactant concentration and aging of the precursor solution, gives rise to an optimized phase separation [66].

Materials

Hybrid organic-inorganic silica films have been prepared by co-hydrolysis in acidic conditions of MTES and TEOS; The precursor solution has been prepared by mixing the following components with respective molar ratios: TEOS : MTES : EtOH : H_2O : HCl = 1 : 0.56 : 4.17 : 1.56 : 2.15x10^{-2}. The precursor sol has been stirred for 45 minutes at 25°C. Three solutions of surfactant has been prepared by dissolving different amounts of Pluronic F127 in 16.5 ml of EtOH and acidic water with molar ratios: EtOH : H_2O : HCl = 1 : 0.32 : 3.32x10^{-4}. The final solution has been prepared by adding 54.2 ml of the precursor sol to the three solutions of surfactant. The amounts of Pluronic F127 has been calculated to obtain the following final molar ratios s = [F127]/[TEOS] = 5x10^{-4}, 1x10^{-3} and 2x10^{-3}.

In order to create also nanocubes in the silica matrix, 3.6 ml of a water solution containing NaCl 0.7 M and Na_2HPO_4 45.5x10^{-3} M have been added to 20 ml of the silica-surfactant sol as the final step (see section 3.2.1). The films have been prepared using the solutions aged at different times: 4, 8 and 12 days; the sols were aged in a closed vessel at 25°C. Hybrid films have been deposited on silicon substrates by dip coating at 25°C, 24% relative humidity (RH) and withdrawal rate of 15 cm/min. After the deposition, films were optically transparent with the exception of the films obtained with the lowest surfactant concentration (s = 5x10^{-4}) which appear opaque. After deposition the films have been treated in an oven in air at 80°C for 12 hours and then at 350°C for 3 hours at atmospheric pressure.

The addition of surfactant and salt to the precursor sol causes the formation of cubes as predicted and, in some specific conditions such as aging time and

surfactant concentration, spherical nano-objects are clearly detectable by TEM measurements. To investigate the nature of these nano-objects, we have combined different analytical techniques.

Structural characterization

The analysis by XRD in grazing incidence, in particular, has shown the presence of only one crystalline phase, shown in figure 3.23, which is clearly attributed to the fcc NaCl.

The formation of salt nanocrystals has been observed only when an aqueous solution of NaCl and Na_2HPO_4 has been used; A necessary condition for the formation of salt precipitates with the shape of nanocubes is, therefore, the addition of an aqueous solution containing both NaCl and Na_2HPO_4. The precipitates that are formed in the film are crystalline sodium chloride, but the presence of the sodium phosphate salt appears necessary for their formation (section 3.2.1). A significant role in the film properties, such as the shape and dimension of pores, is played by the aging time of the solution and surfactant concentration. Systematic experiments have been performed by changing these two parameters while the concentration of the two salts has been maintained constant thanks to the already optimized solution [58].

TEM images in the Figure 3.24 give a direct visualization of the formation of cubic salt precipitates and what we have called *nanospheres*.

The Figure 3.24 shows the TEM images taken from the different samples as a function of sol aging time (increasing aging time from top to bottom) and surfactant concentration (increasing surfactant concentration from left to right). The images show that nanoboxes, whose dimensions are in the range of 100-300 nm, are present in all the samples. Beside the nanoboxes, three of the samples also show the formation of nanospheres with a typical diameter in the range of 50-200 nm. The nanospheres have been observed only in specific conditions of aging and surfactant concentration; in particular, without the addition of the surfactant, no formation of the hollow spheres is visible. The surfactant has also an important role in controlling and stabilizing the formation of the nanocrystals, in fact, without the surfactant we still observed the formation of NaCl nanocrystals, but

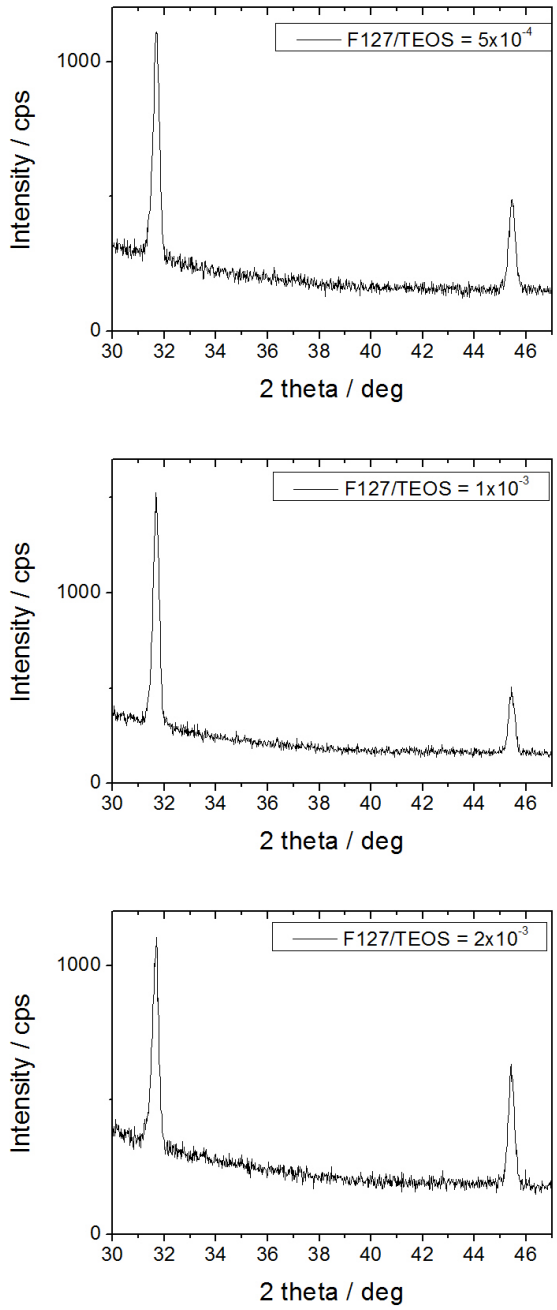

Fig. 3.23: X-ray diffraction patterns of porous thin films deposited using the 4 days aged sols as a function of the [F127]/[TEOS] molar ratio. The patterns show the presence of NaCl face-centered cubic crystals for three different surfactant concentrations.

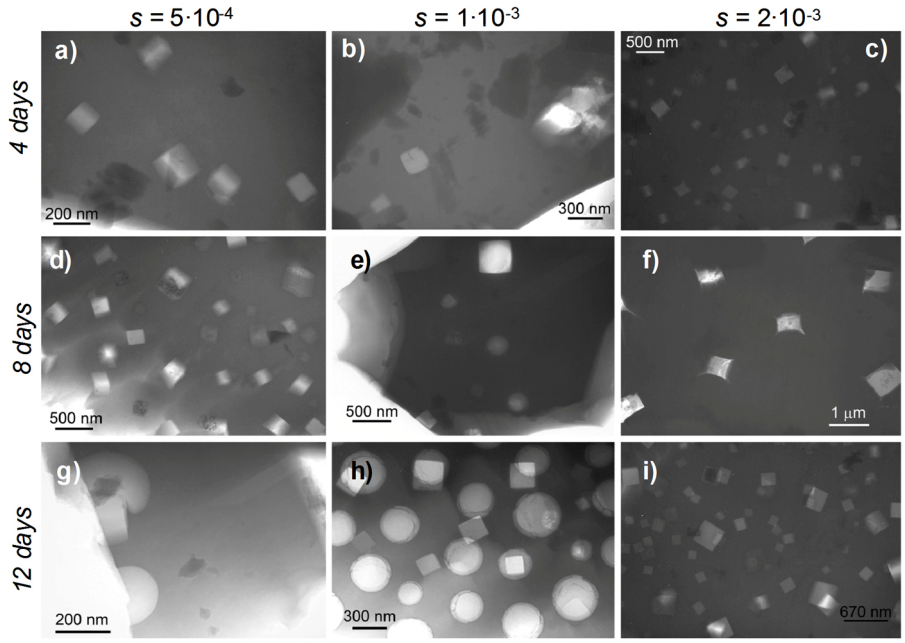

Fig. 3.24: TEM images (a-i) at different magnifications of films treated at 350°C showing different nano-shaped objects. The samples have been prepared by using increasing amount of [F127]/[TEOS] ratio (s) and increasing aging time of the precursors solution. In the three columns from left to right are reported the TEM micrographs of samples having s = $5x10^{-4}$, $1x10^{-3}$ and $2x10^{-3}$, respectively. In the three rows, from top to bottom, are reported the TEM micrographs of samples 4, 8 and 12 days aged, respectively.

the films are opaque. Only when the surfactant has a concentration larger than s = 5x10^{-4} the films are optically transparent.

The types of nanoshape, cubes and/or spheres, which have been observed in every sample is listed in Table 3.3 with the root mean square roughness (R_{rms}) calculated by AFM measurements as a function of solution aging time, and surfactant molar ratio.

Aging time	**[F127]/[TEOS] 5x10^{-4}**	**[F127]/[TEOS] 1x10^{-3}**	**[F127]/[TEOS] 2x10^{-3}**
4 days	Cubes R_{rms} = 22 nm	Cubes R_{rms} = 5.6 nm	Cubes R_{rms} = 3.5 nm
8 days	Cubes R_{rms} = 104 nm	Cubes and Spheres R_{rms} = 83 nm	Cubes R_{rms} = 29 nm
12 days	Cubes and Spheres R_{rms} = 115 nm	Cubes and spheres R_{rms} = 35 nm	Cubes R_{rms} = 10.4 nm

Tab. 3.3: Root mean square roughness (R_{rms}) calculated by AFM measurements as a function of solution aging time and [F127]/[TEOS] molar ratio. The appearance of cubes and/or spheres observed by TEM is reported for every sample.

Electronic diffraction has been used to investigate the nature of nanospheres; no diffraction has been observed in the areas of nanosphere while the presence of crystalline NaCl has been confirmed by diffraction spots from nanoboxes. The nature of the two objects appears, therefore, quite different and also their shape gives some important indications; the inorganic salt crystals produce nanocubes because of the crystallographic structure of sodium chloride, but they can not template pores with spherical shape. It's reliable that the nanospheres are hollow areas formed by solvent phase separation and evaporation during film deposition.

The thickness of the films in the different conditions of sol aging and surfactant concentration has been calculated by ellipsometric spectroscopy; the results are shown in Figure 3.25. The ellipsometric spectra were recorded in the 400-900 nm range; data analysis was done assuming a Cauchy film as fitting model which calculates the refractive index as a function of the wavelength: $n(\lambda) = A + B/\lambda^2 + C/\lambda^4$. Fitting parameters were A, B, C together with the film thickness. The graph shows a 3D plot of thickness versus aging time and surfactant concentration,

the thickness is reported in a false colors scale. The thickness changes between around 0.6 and 1 μm; as a general trend higher contents of surfactant and longer aging times produce thicker coatings.

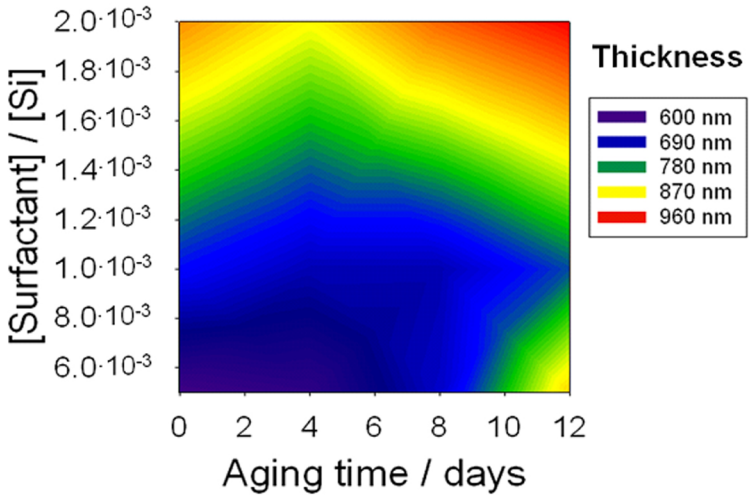

Fig. 3.25: 3D plot (aging time - surfactant concentration - thickness) of film thickness after thermal treatment at 350°C as a function of surfactant and aging time. The thickness change is indicated by the false color scale.

The films surface area has been characterized by optical microscopy and atomic force microscopy in order to find a correlation between the surface morphology and the inner porousity. The optical images of films in Figure 3.26 show that the surface changes with the composition and aging time in a very sensitive way. We observe a direct correlation between this change and the formation of nano-objects of different dimensions within the films. The images in Figure 3.26 show that the dimensions of the surface irregularities decrease with the increasing of the surfactant concentration while an increase of the sol aging favors the formation of larger irregularities.

The images of the different samples as a function of surfactant concentration and aging time obtained by atomic force microscopy are shown in Figure 3.27.

The AFM images are in good agreement with the optical images and show a similar trend; a higher content of surfactant and a shorter aging time reduce the

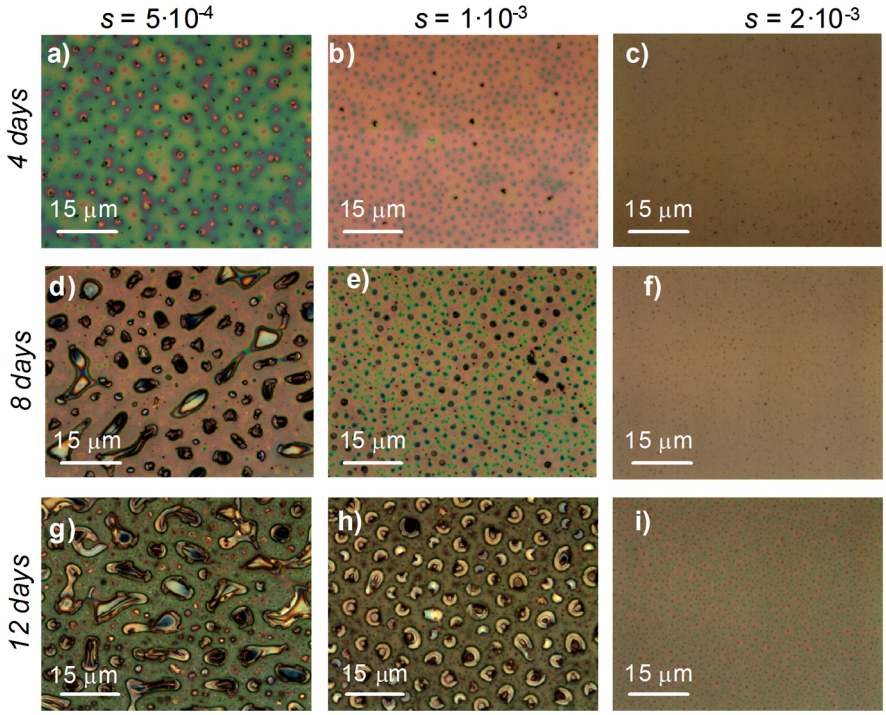

Fig. 3.26: Optical microscopy images of the film surfaces after thermal treatment at 350°C as a function of the [F127]/[TEOS] ratio (s) and aging time of the precursors sol. In the three columns, from left to right, are reported the optical micrographs of samples having s = $5x10^{-4}$, $1x10^{-3}$ and $2x10^{-3}$, respectively. In the three rows, from top to bottom, are reported the images of samples 4, 8 and 12 days aged, respectively.

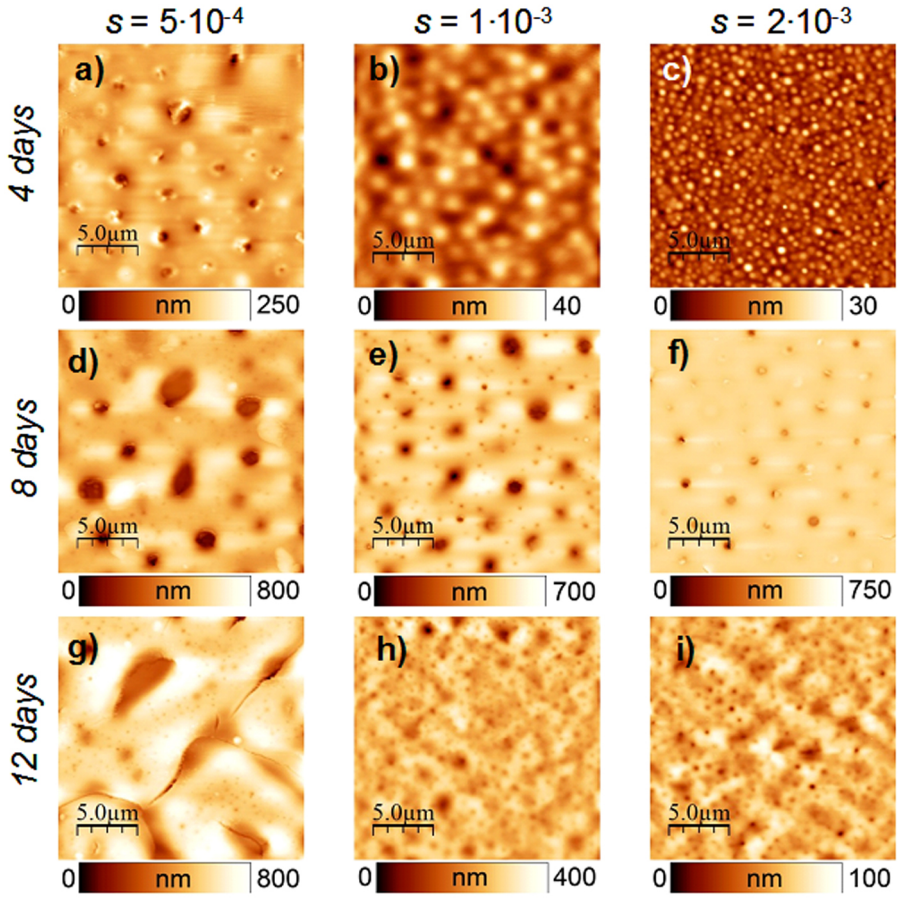

Fig. 3.27: AFM images of the film surfaces after thermal treatment at 350°C as a function of the [surfactant]/[Si] ratio (s) and aging time (a) of the precursors solution. The three columns from left to right are reporting the images of samples having s = $5x10^{-4}$, $1x10^{-3}$ and $2x10^{-3}$ respectively while the three rows, from the top to the bottom, are reporting the images of samples aged a = 4, 8 and 12 days, respectively.

R_{rms} of the film surface as described in Table 3.3. The AFM images have been also used to obtain a statistical evaluation of the surface morphology and the results are shown in Figure 3.28. Root mean square roughness R_{rms} and average height h_a have been calculated and roughness analysis histograms is plotted in Figure 3.28. R_{rms} is calculated through the formula:

$$R_{rms} = \sqrt{\frac{1}{MN}\sum_{i=1}^{M}\sum_{j=1}^{N} z^2}$$

where MN is the image area (columns multiplied by rows) and z is the measured sample height in each point of the area. Histograms show the sample height on X axis and probability on Y axis; the X axis in each plot has been rescaled with respect to the average height, h_a.

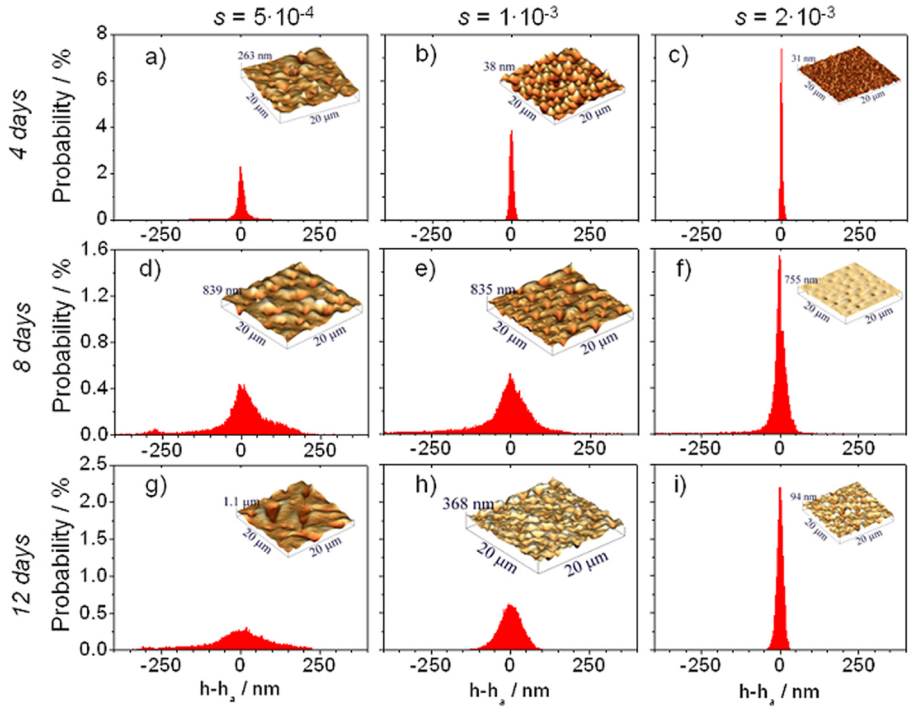

Fig. 3.28: Roughness analysis of the AFM images in Figure 3.27; the insets are AFM 3D views of the corresponding films surface. The X scale shows the h(height) - ha(average height) value expressed in nm.

The histograms show that the amplitude of undulation increases with aging time of solution while decreases with the increase of surfactant concentration. This means that longer aging times produce a surface with higher variations of valleys and peaks height, as indicated by an enlargement of the distribution curve of h-h_a. On the other hand, an increase of surfactant concentration allows obtaining smoother surfaces as shown by the sharpening of the curve. If, therefore, we consider only the effects of the different processing parameters, the surfactant plays a dominant role on surface smoothing; in fact at high surfactant concentrations (s = 2x10^{-3}) the full width at half maximum of the h-h_a curve is less affected by the aging of the sol.

Chemical characterization

Infrared spectroscopy in the middle infrared range (4000-400 cm^{-1}) has been used to evaluate the effect of aging on the hybrid structure and in the far-infrared (400-30 cm^{-1}) range to study the formation of NaCl nanocrystals. Figure 3.29 shows the FTIR absorption spectra in the 1320-900 cm^{-1} range of the as-deposited samples as a function of surfactant concentration (increasing surfactant concentration from left to right) and aging time (increasing aging time from top to bottom) of the precursor sol.

The spectra show a sharp band of small intensity peaking at 1290 cm^{-1} which is assigned to Si-CH_3 vibration and is taken as a signature of the presence of methyl groups in the hybrid films. Around 1100 cm^{-1} a wide band is observed which is due to Si-O-Si antisymmetric stretching, at the lowest aging times (Figure 3.29 a, b and c) another overlapped band is also observed; this band is assigned to the presence of unreacted Si-OR groups [55]. The same attribution is done for the band at 920 cm^{-1} which is observed in the same samples and that is overlapping the Si-OH band at 900 cm^{-1}. The disappearing of these bands at higher aging times indicates that the hybrid network is more interconnected in the films obtained from sols aged more than 4 days.

The absorption spectra in the 195-155 cm^{-1} of porous organic-inorganic hybrid films prepared by using increasing amounts of surfactant and increasing aging times are reported in Figure 3.30. Figures 3.30 a, b, and c show the spectra of

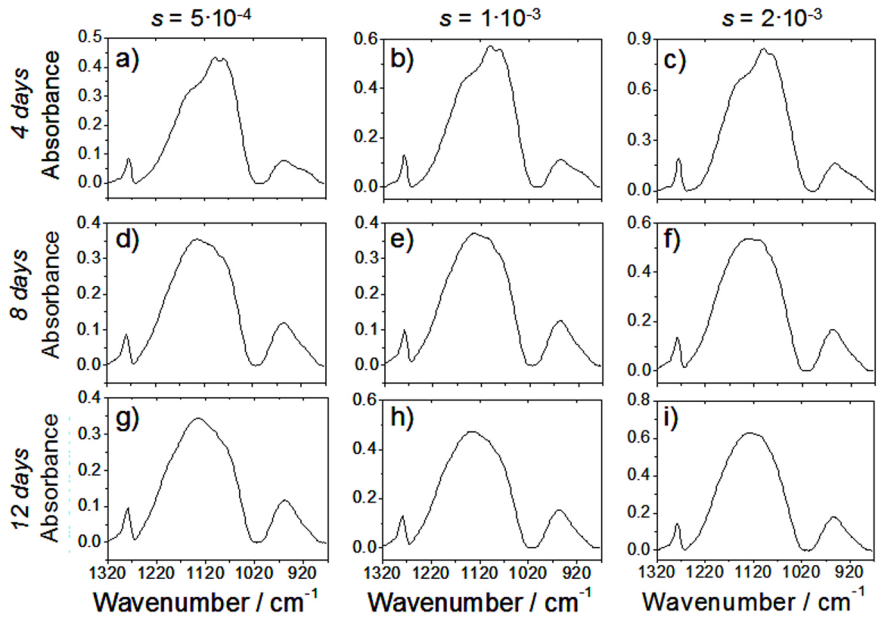

Fig. 3.29: FTIR absorption spectra in the 1320-900 cm^{-1} range of as deposited organic-inorganic hybrid films prepared by using increasing amounts of [surfactant]/[Si] ratio (s) and increasing aging time (a) of the precursors sol. In the three columns, from left to right, are reported the spectra of samples with s = $5x10^{-4}$, $1x10^{-3}$ and $2x10^{-3}$, respectively. In the three rows, from the top to the bottom, are reported the spectra of samples aged a = 4, 8 and 12 days respectively.

the samples with s = 5x10^{-4}, 1x10^{-3} and 2x10^{-3}, respectively.

In the three figures the solid black, red and green lines are referred to films deposited from precursor sols aged for 4, 8 and 12 days, respectively; the dot blue line shows the spectrum of *bulk* sodium chloride with crystal dimensions larger than 200 nm. As a general trend, the spectra of the samples are composed by two overlapped absorption curves, one peaking around 165 cm^{-1} and another around 180 cm^{-1}. The two bands change in relative intensity in the different samples; the main effect appears related to the surfactant concentration because at the highest s value, the band at 180 cm^{-1} has the highest intensity. To discuss the origin and change of these two bands, we can take as reference the spectrum of *bulk* sodium chloride. This is formed by a single wide absorption band centered around 162 cm^{-1}, a shift from this value to higher wavenumbers (Figure 3.30 a) can be attributed to a decrease in dimension of the salt crystals. Interestingly we do not observe only a shift of the 165 cm^{-1} phononic vibration, but also a rise of the other band at higher wavenumbers. This band is assigned to phononic modes of smaller sodium chloride nanocubes. The attribution has to be taken with caution, because we could not get unambiguous data from TEM observations to support a bimodal distribution of salt nanocrystals.

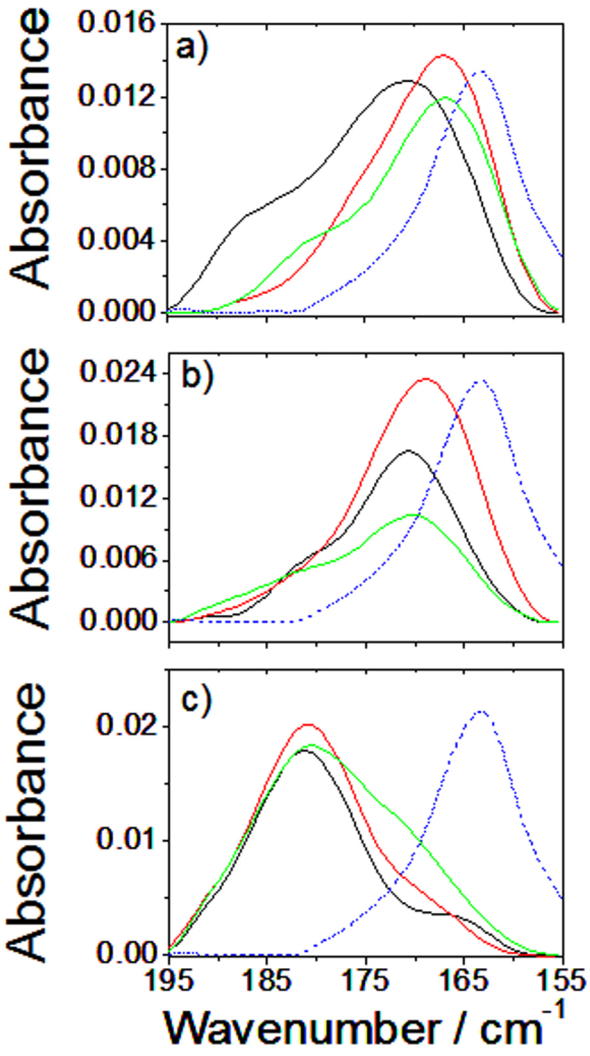

Fig. 3.30: Far infrared absorption spectra in the 195-155 cm^{-1} interval of organic-inorganic hybrid films surfaces after thermal treatment at 350°C and prepared by using increasing amounts of [surfactant]/[Si] ratio (s) and increasing aging time (a) of the precursors sol. Figures a, b, and c are referred to samples with s = $5x10^{-4}$, $1x10^{-3}$ and $2x10^{-3}$, respectively. In the three figures the solid black, red and green lines are referred to films deposited from precursors solutions aged for 4, 8 and 12 days, respectively. The blue dot line is the crystalline NaCl.

Chapter 4

Conclusions and perspective

The synthesis of thin films with pores of different shape, dimension and topological distribution of nano-objects opens important perspectives in different fields of application, such as sensing and nanobiotechnologies. The presence of gold nanoparticles at the interface between a biological analyte and the porous matrix, in fact, should allow a strong increase in the detection signal due to a collective oscillation of conduction electrons of the metal nanoparticles (plasmon).

In this doctorate work, the leading trend was to make a step ahead in the chemical and structural design for new highly functional materials. The aim of this work was to succeed in controlling size and shape of meso-macro scale hierarchal structures in order to expand the possibility for realizing multi-functional materials. At the same time, the first step in the practical application process has been achieved, by the use of a patterning technique, to the mesoporous thin films not just as a patterning process but as a tool to obtain multiple effects and properties in the film.

A new sol-gel synthesis route has been developed that allows the formation of two types of pore templates during the solvent evaporation, spherical micelles from block copolymers and crystalline nanoboxes from salts (NaCl). Formation of NaCl nanocrystals is driven by the evaporation of the solvent during film deposition while uncontrolled precipitation of the salt is avoided by the coaddition of Na_2HPO_4 in the precursor sol. The removal of the template can be done in a selective way: block copolymers are eliminated by thermal treatment and

salt nanoboxes are removed by a simple water washing of the film. The final material appears as a porous hierarchical film with two ranges of porosities, an ordered array of mesopores, and cubic nanoboxes in the range 120-280 nm from the salt nanocrystals. This method will allow a selective functionalization of the nanopores through a controlled multi-step process. The possibility of following in situ the hierarchical film formation by simultaneous time resolved analytical techniques has allowed to get a better in sight of the evaporation driven processes with different templates. The role of two different templates during film processing giving pores of different dimensions, in the meso and macro range, has been completely understood.

Another kind of interesting porous material has been obtained during this doctorate work by a modification and aging of the precursor solution. Salt nanocrystals and hollow nanospheres have been obtained within the films as a function of the processing conditions. In this case surfactant, salt concentration and aging time are all critical parameters that affect the formation of nano-objects, also the surfactant plays an important role. Two different phenomena appear involved in the formation of nano-objects with two distinct shapes: the precipitation of NaCl crystals and the solvent phase separation. The first process is driven by the evaporation of the solvent during the film deposition as in hierarchical thin films; the salt precipitation is controlled by the co-addition of the second salt which changes the solubility during evaporation of the solvents and eventually favors the nucleation of the nano-crystals. The surfactant plays also a crucial role because helps to stabilize the process and control the dimension of the precipitates. The second process leads to the formation of the hollow nanospheres. This process is much more difficult to control and, in fact, is observed only at specific surfactant concentration and aging time.

On the other hand an integrated combination of top-down and bottom-up technologies has been used to fabricate a complex multi-functional nanomaterial. Deep X-ray lithography has been used on mesoporous materials as an alternative route to give new functionalities to the film. X-rays coming from a synchrotron radiation induce condensation of the pore walls, remove the surfactant and partially remove the covalently bonded organic groups in a TEOS-MTES mesoporous film.

At the same time, in presence of a gold precursor in the solution, gold nanoparticles are formed in a simple and controlled way. The X-ray dose controls the process. The exposed part of the film is selectively condensed by X-rays thus allowing a very effective chemical etching and the fabrication of high-aspect-ratio patterns, with sharp walls and low surface roughness. The process appears to be direct, highly reproducible, and does not need several complicate steps for the fabrication of complex porous patterns which contain nanoparticles of controlled dimensions.

This doctorate work sets in a wider context regarding the obtaining of nano-bio devices (such as sensors and lab-on-a-chip) by the integrated approach of bottom-up and top-down techniques. So far, novel complex porous materials in the form of thin films have been obtained with a strict control of pore shape, size and accessibility. Also a method for obtaining a highly reproducible gold nanoparticles embedded in a mesoporous matrix has been developed giving rise to a useful SERS effect. Next step is to integrate all the knowledge in the construction of a unique device able to easily detect biological species of different size and function at the same time.

This doctorate work has been carried out in the Laboratory of Materials and NanoTecnologies (LMNT) of University of Sassari.

Bibliography

[1] The Royal Society, *Nanoscience and nanotechnologies: opportunities and uncertainties*, The Royal Society & The Royal Academy of Engineering (2004).

[2] P. Falcaro, S. Costacurta, L. Malfatti, M. Takahashi, T. Kidchob, M.F. Casula, M. Piccinini, A. Marcelli, B. Marmiroli, H. Amenitsch, P. Schiavuta, and Plinio Innocenzi, *Adv. Mater.*, **20**, 1864 (2008).

[3] B.D. Gates, Q. Xu, M. Stewart, D. Ryan, C.G. Willson, G.M. Whitesides, *Chem. Rev.*, **105**, 1171 (2005).

[4] J.Y. Cheng, C.A. Ross, H.I. Smith, E.L. Thomas, *Adv. Mater.*, **18**, 2505 (2006).

[5] J. Rouquerol, D. Avnir, C.W. Fairbridge, D.H. Everett, J.H. Haynes, N. Pericone, J.D.F. Ramsay, K.S.W. Sing, K.K. Unger , *Pure Appl. Chem.*, **66**, 1739 (1994).

[6] H. Craighead, *Nature*, **442**, 387 (2006).

[7] P. Persans, M. Tomozawa, J.L. Plawsky, E. Simonyi, *Thin Solid Films*, **513**, 398 (2001).

[8] S. Baskaran, J. Liu, K. Domansky, N. Kohler, X. Li, C. Coyle, G.E. Fryxell, T. Suntharampillai, R.E. Williford, *AdV. Mater.*, **12**, 291 (2000).

[9] A.R. Balkenende, F.K. de Theije, J.C. Kriege, *AdV. Mater.*, **15**, 139 (2003).

[10] C.J. Brinker, Y. Lu, A. Sellinger, H. Fan, *Adv. Mater.*, **11**, 579 (1999).

[11] N. Liu, D.R. Dunphy, P. Atanassov, S.D. Bunge, Z. Chen, G.P. Lopez, T.J. Boyle, and C.J. Brinker, *Nano Lett.*, **4**, 551 (2004).

[12] a) C.T Kresge, M.E. Leonowicz, W.J. Roth, J.C. Vartuli, J.S. Beck, *Nature* **359**, 710 (1992). b) J.S. Beck, J.C. Vartuli, W.J. Roth, M.E. Leonowicz, C.T. Kresge, K.D. Schmitt, C.T.W. Chu, D.H. Olson, E.W. Sheppard, S.B. McCullen, J.B. Higgins, J.L. Schlenker, *J. Am. Chem. Soc.*, **114**, 10834 (1992).

[13] M. Ogawa *J. Am. Chem. Soc.*, **116**, 7941-7942 (1994).

[14] H. Yang, N. Coombs, I. Sokolov, G.A. Ozin, *Nature*, **381**, 589 (1996).

[15] H. Yang, A. Kuperman, N. Coombs, S. Mamiche-Afara, G.A. Ozin, *Nature*, **379**, 703 (1996).

[16] Y. Lu, H. Fan, A. Stump, T.L. Ward, T. Rieker, C.J. Brinker, *Nature*, **398**, 223 (1999).

[17] N.A. Melosh, P. Lipic, S.F. Bates, F. Wudl, G.D. Stucky, G.H. Fredrickson, B.F. Chmelka, *Macromolecules*, **32**, 4332 (1996).

[18] S. De Paul, J.W. Zwanziger, R. Ulrich, U. Wiesner, H.W. Spiess, *J. Am. Chem. Soc.*, **127**, 5727 (1996).

[19] A.C. Finnefrock, R. Ulrich, A. Du Chesne, C. Honeker, K. Schumacher, K.K. Unger, S. Gruner, U. Wiesner, *Angew. Chem. Int. Ed.*, **40**, 1208 (2001).

[20] M. Templin, A. Franck, A. Du Chesne, H. Leist, Y. Zhang, R. Ulrich, V. Schadler, U.Wiesner, *Science*, **278**, 1795 (1997).

[21] P.F. Simon, R. Ulrich, H.W. Spiess, U. Wiesner, *Chem. Mater.*, **13**, 3464 (2001).

[22] R.K. Iler, *The Chemistry of Silica*, Wiley, New York, (1979).

[23] P. Falcaro, S. Costacurta, G. Mattei, H. Amenitsch, A. Marcelli, M. Cestelli Guidi, M. Piccinini, A. Nucara, L. Malfatti, T. Kidchob, P. Innocenzi, *J. Am. Chem. Soc.*, **127**, 3838 (2005).

[24] G.A. Ozin, *Nature*, 379, (1996).

[25] G.A. Ozin, H. Yang, N. Coombs, *Nature*, **381**, 589 (1996).

[26] P.J. Bruinsma, A.Y. Kim, J. Liu, S. Baskaran, *Chem. Mater.*, **9**, 2507 (1997).

[27] G.J. de A.A. Soler-Illia, C. Sanchez, B. Lebeau, and J. Patarin, *Chem. Rev.*, **102**, 4093 (2002).

[28] L.E. Scriven in *Better Ceramics Through Chemistry III* eds. C.J. Brinker, D.E. Clark, D.R. Ulrich Materials Research Society in Pittsburgh, PA, (1988).

[29] P. Yang, T. Deng, D.Y. Zhao, P. Feng, D. Pine, B.F. Chmelka, G.M. Whitesides, G.D. Stucky, *Science*, **282**, 2244 (1998).

[30] Kazuki Nakanishi, *Journal of Porous Materials*, **4**, 67-112 (1997).

[31] D. Zhao, P. Yang, B.F. Chmelka, G.D. Stucky, *Chem. Mater.*, 11, 1174 (1999).

[32] B.T. Holland, C.F. Blanford, A. Stein, *Science*, **281** 538, (1998).

[33] M. Antonietti, B. Berton, C Goltner, H.-P. Hentze, *Adv. Mater.*, **10** 154, (1998).

[34] T. Sen, G.J.T. Tiddy, J.L. Casci, and M.W. Anderson, *Angew. Chem. Int. Ed.*, **42**, 4649 (2003).

[35] C.J. Brinker, D.R. Dunphy, *Curr. Opin. Colloid Interface Sci.*, **11**, 126 (2006).

[36] D.A. Doshi, N. Huesing, M. Lu, H. Fan, Y. Lu, K. Simmons-Potter, B.G. Potter Jr, A.J. Hurd, C.J. Brinker,, *Science*, **290**, 107 (2000).

[37] H. Fan, Y. Lu, A. Stump, S.T. Reed, T. Baer, R. Schunk, V. Perez-Luna, G.P. Lopez, C.J. Brinker, *Nature*, **405**, 56 (2000).

[38] P. Innocenzi, T. Kidchob, P. Falcaro, M. Takahashi, *Chem. Mater.*, **20**, 607 (2008).

[39] Y.N. Xia and G.M. Whitesides, *Annu. Rev. Mat. Sci.*, **28** 153 (1998).

[40] M. Trau, N. Yao, E. Kim, Y. Xia, G.M. Whitesides, I.A. Aksay, *Nature*, **390** 674 (1997).

[41] T. Ito, S. Okazaki, *Nature*, **406** 1027 (2000).

[42] G. Della Giustina, M. Prasciolu, G. Brusatin, M. Guglielmi, F. Romanato, *Mater. Sci. Eng. C*, **27** 1382 (2007).

[43] P. Meyer, J. Schulz, L. Hahn, V. Saile, *Microsyst. Technol.*, **14** 1491 (2008).

[44] W. Ehrfeld, V. Hessel, H. Lowe, C. Schulz, L. Weber, *Microsyst. Technol.*, **5** 105 (1999).

[45] R.K. Chang and T.E. Furtak, *Surface-Enhanced Raman Scattering*, New York (1982).

[46] N. Anderson, A. Hartshuh, L. Novotny, *Mater. Today*, **5**, 50 (2005)

[47] A. Wokaun *Solid State Phys.*, **38**, 223 (1984)

[48] L. Malfatti, D. Marongiu, S. Costacurta, P. Falcaro, H. Amenitsch, B. Marmiroli, G. Grenci, M.F. Casula, and P. Innocenzi, *Chem. Mater.*, **22**, 2132 (2010).

[49] Barbara H. Stuart, *Infrared Spectroscopy: Fundamentals and Applications*, Wiley (2004).

[50] V. L. Mironov, *Fundamentals of Scanning Pbobe Microscopy*, The Russian Academy of sciences institute for physics of microstructures (2004).

[51] J. Belloni, M. Mostafavi, H. Remita, J.H. Marignier, M.O. Delcourt, *New J. Chem.*, 1239Ű1255 (1998).

[52] C.H. Wang, T.E. Hua, C.C. Chien, Y.L. Yu, T.Y. Yang, C.J. Liu, W.H. Leng, Y. Hwua, Y.C. Yang, C.C. Kim, J.H. Je, C.H. Chen, H.M. Lin, G. Margaritondo, *Mater. Chem. Phys.*, **106**, 323Ű329, (2007).

[53] E. Gachard, H. Remita, J. Khatouri, B. Keita, L. Nadjo, J. Belloni, *New J. Chem.*, 1257Ű1265 (1998).

[54] N.B. Colthup, L.H. Daly, S.E. Wiberley, *Introduction to Infrared and Raman Spectroscopy*, Academic Press, Boston (1990).

[55] P. Innocenzi, *J. Non-Cryst. Solids*, **316**, 309 (2003).

[56] W. Haiss, N.T.K. Thanh, J. Aveyard, D.G. Fernig, *Anal. Chem.*, **79**, 4215 (2007).

[57] N. Felidj, J. Aubard, G. Levia, J.R. Krenn, A. Hohenau, G. Schider, A. Leitner, F.R. Aussenegg, *Appl. Phys. Lett.*, **82**, 3095 (2003).

[58] L. Malfatti, P. Falcaro, D. Marongiu, M.F. Casula, H. Amenitsch, and P. Innocenzi, *Chem. Mater.*, **21**, 4846 (2009).

[59] P. Falcaro, S. Costacurta, G. Mattei, H. Amenitsch, A. Marcelli, M. Cestelli Guidi, M. Piccinini, A. Nucara, L. Malfatti, T. Kidchob, P. Innocenzi, *J. Am. Chem. Soc.*, **127**, 3838 (2005).

[60] P. Falcaro, D. Grosso, H. Amenitsch, P. Innocenzi, *J. Phys. Chem. B*, **108**, 10942 (2004).

[61] L. Malfatti, T. Kidchob, P. Falcaro, S. Costacurta, M. Piccinini, M. Cestelli Guidi, A. Marcelli, A. Corrias, M.F. Casula, H. Amenitsch, P. Innocenzi, *Microporous Mesoporous Mater.*, **103**, 113 (2007).

[62] L. Malfatti, D. Marongiu, H. Amenitsch, P. Innocenzi, *Submitted to The Journal of Physical Chemistry.*

[63] M.P. Tate, V.N. Urade, J.D. Kowalski, T.C. Wei, B.D. Hamilton, B.W. Eggiman, and H.W. Hillhouse, *J. Phys. Chem. B*, **110**, 9882 (2006).

[64] P. Innocenzi, L. Malfatti, T. Kidchob, P. Falcaro, S. Costacurta, M. Guglielmi, G. Mattei, H. Amenitsch, *J. Synch. Rad.*, **12**, 734 (2005).

[65] X. Jiang, C.J. Brinker, *J. Am. Chem. Soc.*, **128**, 4512 (2006).

[66] P.Innocenzi, L. Malfatti, D. Marongiu, M.F. Casula, *submitted to New Journal of Chemistry.*

Publications related to doctorate

- Luca Malfatti, Daniela Marongiu, Heinz Amenitsch, Plinio Innocenzi *'Simultaneous in situ and time-resolved study of hierarchical porous films templated by salt nanocrystals and self-assembled micelles'*, submitted to *The Journal of Physical Chemistry.*

- Plinio Innocenzi, Luca Malfatti, Daniela Marongiu, Maria F. Casula *'Controlling shape and dimensions of pores in organic-inorganic films: nanocubes and nanospheres'*, submitted to *New Journal of Chemistry.*

- Luca Malfatti, Daniela Marongiu, Stefano Costacurta, Paolo Falcaro, Heinz Amenitsch, Benedetta Marmiroli, Gianluca Grenci, Maria Francesca Casula, and Plinio Innocenzi *'Writing Self-Assembled Mesostructured Films with In situ Formation of Gold Nanoparticles'*, *Chem. Mater.* **2010**, 22, 2132-2137

- Luca Malfatti, Paolo Falcaro, Daniela Marongiu, Maria F. Casula, Heinz Amenitsch, and Plinio Innocenzi *'Self-Assembly of Shape Controlled Hierarchical Porous Thin Films: Mesopores and Nanoboxes' Chem. Mater.* **2009**, 21, 4846-4850.

Other publications

- Tongjit Kidchob, Luca Malfatti, Daniela Marongiu, Stefano Enzo, Plinio Innocenzi *'An alternative sol-gel route for the preparation of thin films in CeO_2-TiO_2 binary system'*, *Thin Solid Films* **2010**, 518, 1653-1657.

- Tongjit Kidchob, Luca Malfatti, Daniela Marongiu, Stefano Enzo, Plinio Innocenzi *'Formation of cerium titanate, CeTi2O6, in solŰgel films studied by XRD and FAR infrared spectroscopy'*, *J. Sol-Gel Sci. Technol.* **2009**, 52, 356-361.

- Alberto Calloni, Rafael Ferragut, Fabio Moia, Alfredo Dupasquier, Giovanni Isella, D. Marongiu, Gerd Norga, Alexey Fedorov, and Danny Chrastina *'Positron annihilation studies of defects in $Si_{1-x}Ge_x$/SOI heterostructures'*, *Phys. Status Solidi C* **2009**, 6, No. 11, 2304-2306.